Quantum state inference from coarse-grained descriptions: Analysis and an application to quantum thermodynamics

Raúl O. Vallejos [1,*] Pedro Silva Correia,[2] Paola Concha Obando [1] Nina Machado O'Neill,[1]
Alexandre B. Tacla,[1] and Fernando de Melo [1,†]

[1]*Centro Brasileiro de Pesquisas Físicas (CBPF), Rua Doutor Xavier Sigaud 150, 22290-180 Rio de Janeiro, Brazil*
[2]*Instituto de Física, Universidade Federal Fluminense, Av. Gal. Milton Tavares de Souza s/n, Gragoatá 24210-346, Niterói, RJ, Brazil*

The characterization of physical systems relies on the observable properties which are measured, and how such measurements are performed. Here we analyze two ways of assigning a description to a quantum system assuming that we only have access to coarse-grained properties. More specifically, we compare the maximum entropy principle method, with the Bayesian-inspired recently proposed average assignment map method [Correia *et al.*, Phys. Rev. A **103**, 052210 (2021)]. Despite the fact that the assigned descriptions by both methods respect the measured constraints, and that they share the same conceptual foundations, the descriptions differ in scenarios that go beyond the traditional system-environment structure. The average assignment map is thus shown to be a more sensible choice for the ever more prevalent scenario of complex quantum systems. We discuss the physics behind such a difference, and further exploit it in a quantum thermodynamics process.

I. INTRODUCTION

Whether considering our everyday perception of the surrounding environment or a sophisticated experimental setup, a characterization of a physical system is given in terms of measurement results of its observable properties. The characterization of a physical system is thus not unique: aside from considering *which* features are being observed, it is also necessary to take into account *how* these features are being observed.

For the first consideration, the "which features" part, given a set of observed properties, say a set $\mathcal{O} = \{o_i\}$ of expected values o_i, the objective of state inference is to assign to the system a description that abides by the known data. However, more often than not, the number of constraints is not sufficient to single out a unique state for the system, i.e., there are many states which are compatible with the known data. Let $\Omega(\mathcal{O})$ be the set of all descriptions which are consistent with the knowledge about the system. Back all the way to Laplace's principle of indifference, it is only reasonable to appoint the same probability for each description in $\Omega(\mathcal{O})$, and to assign the average description $\overline{\Omega(\mathcal{O})}$ to the system. The use of the maximum entropy principle (MEP) [1,2], i.e., to assign to the system the description in $\Omega(\mathcal{O})$ which has the maximum Shannon entropy, made this intuitive idea more mathematically concrete, allowing for the inclusion of constraints and symmetries, and extending its reach to continuous sets. The MEP has found applications in fields as diverse as biology, computer science, and financial markets [3–11]. Within physics, the MEP received a great deal of attention

as it recovers the ensembles of statistical physics [12]. The same success is observed in the quantum realm, where one now assigns to the system the quantum state that maximizes the von Neumann entropy, while respecting the known constraints [13,14].

Concerning "how" features are measured, most inference methods, and the MEP in particular, are somewhat reticent. For quantum systems, which are the subject of the present contribution, the only point which is systematically taken care of is the locality of the observables. Consider, for instance, the scenarios described by the theory of open quantum systems [15,16]. In such a case it is possible to split the total system into two parts: the system of interest S, which we assume to have access to, and the environment E, whose degrees of freedom we have no control of. Aside from a possible restriction on the full system (like the total energy), when inferring the total system description, one usually only knows about local properties of the system.

More concretely, associate to the total system a Hilbert space $\mathcal{H}_S \otimes \mathcal{H}_E$, and assume that we know the expected values for a set $\mathcal{O}$ of subsystem S properties. Quantum mechanics tells us that there exists a set of observables $\{O_i\}$ and a density matrix ϱ_S, acting on $\mathcal{H}_S$, such that $o_i = \text{tr}(O_i \varrho_S)$ for all $i \in \{1, \ldots, |\mathcal{O}|\}$. As the total system lives in $\mathcal{L}(\mathcal{H}_S \otimes \mathcal{H}_E)$, with $\mathcal{L}(\mathcal{H})$ representing the set of linear operators acting on $\mathcal{H}$, the reduced density matrix ϱ_S is obtained from the total one ϱ_{SE} by "tracing out" system E degrees of freedom, i.e., $\varrho_S = \Lambda_{\text{tr}_E}[\varrho_{SE}]$. Here, the map $\Lambda_{\text{tr}_E} : \mathcal{L}(\mathcal{H}_S \otimes \mathcal{H}_E) \mapsto \mathcal{L}(\mathcal{H}_S)$ is the partial-trace map. If one wants to assign a description to the total system, the local constraints can be extended to the full system as follows:

$$o_i = \text{tr}\big(O_i\, \Lambda_{\text{tr}_E}[\varrho_{SE}]\big) = \text{tr}\big(\Lambda^*_{\text{tr}_E}[O_i]\, \varrho_{SE}\big) = \text{tr}(O_i \otimes \mathbb{1}_E\, \varrho_{SE}).$$

*vallejos@cbpf.br
†fmelo@cbpf.br

In the above, $\Lambda^*_{\mathrm{tr}_E} : \mathcal{L}(\mathcal{H}_S) \mapsto \mathcal{L}(\mathcal{H}_S \otimes \mathcal{H}_E)$ is the trace-dual map associated to the partial-trace operation, which only augments the observable with the identity matrix in the E sector. One can now use an inference method to assign a description of the total system, which should abide by the constraints $o_i = \mathrm{tr}(O_i \otimes \mathbb{1}_E \, \varrho_{SE})$ for all $i \in \{1, \ldots, |\mathcal{O}|\}$.

However, with the control of quantum systems reaching unprecedented levels, as driven by the development of modern quantum technologies, a new scenario comes forth. In this new picture, highly isolated complex quantum systems are produced whose microscopic description is experimentally challenging, requiring single-particle addressing, and theoretically hopeless, due to the exponential increase of system dimension with the number of particles. In this new scenario, not only the observed data are local, but also stems from an effective description of the system.

In order to deal with this new class of phenomena, quantum channels with the output dimension smaller than the input dimension, dubbed coarse-graining channels, were used to obtain a system's effective description [17–31]. In this formalism, a coarse-graining map is thus a completely positive map $\Lambda : \mathcal{L}(\mathcal{H}_D) \mapsto \mathcal{L}(\mathcal{H}_d)$ such that $\dim(\mathcal{H}_D) > \dim(\mathcal{H}_d)$. Very much like the partial-trace map, the output description has fewer degrees of freedom than the total description. Differently from the partial trace, general coarse-graining maps do not require a clear-cut split between system and environment, being thus more appropriate to effectively describe complex highly interacting isolated quantum systems. See Fig. 1 for an example of effective description possible to be characterized by general coarse-graining maps, and how it differs from the usual partial-trace situation.

In the proposed framework, suppose that to a system's effective description we associate a Hilbert space $\mathcal{H}_d$, and that we know the expected values for a set $\mathcal{O}$ of effective properties. As before, there exists a set of observables O_i and a density matrix ϱ_d, in $\mathcal{L}(\mathcal{H}_d)$, such that $o_i = \mathrm{tr}(O_i \varrho_d)$ for all $i \in \{1, \ldots, |\mathcal{O}|\}$. Since ϱ_d is an effective description, we can assume that it is the result of a coarse-graining map acting on a microscopic description $\varrho_D \in \mathcal{L}(\mathcal{H}_D)$, i.e., $\varrho_d = \Lambda[\varrho_D]$. If we want to infer the microscopic description, we can extend the known constraints as previously:

$$o_i = \mathrm{tr}(O_i \, \Lambda[\varrho_D]) = \mathrm{tr}(\Lambda^*[O_i] \, \varrho_D).$$

In the above, $\Lambda^* : \mathcal{L}(\mathcal{H}_d) \mapsto \mathcal{L}(\mathcal{H}_D)$ is the trace-dual map associated with the coarse-graining channel map Λ. These constraints can now be included in an inference method to obtain a microscopic description that abides by the coarse-grained data.

While in principle one could use the MEP to assign a description to the microscopic state, when studying the effective dynamics that might emerge from a coarse-grained dynamics [32], an assignment map naturally surfaced. Consider the set of all states which are consistent with the coarse-grained data, i.e., the set

$$\Omega_\Lambda(\mathcal{O}) = \{\psi \in \mathcal{L}(\mathcal{H}_D) \mid \mathrm{tr}(O_i \Lambda[\psi]) = o_i,$$
$$\forall \, i \in \{1, \ldots, |\mathcal{O}|\}\}. \tag{1}$$

As in the foundations of the MEP, in Ref. [32] it was suggested to assign to the underlying system the description

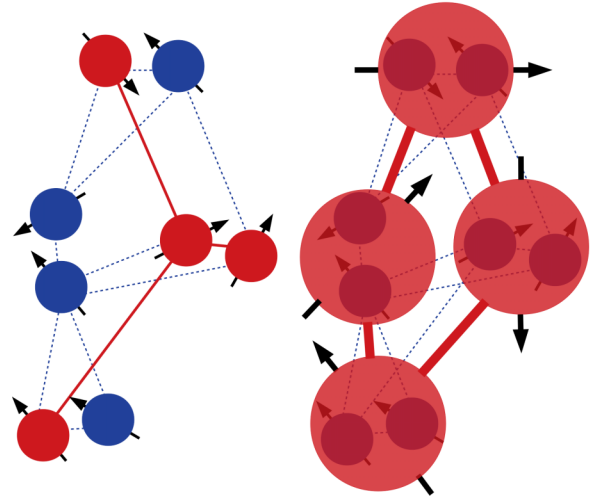(a) Open quantum system   (b) Generalized coarse-grained scenario

FIG. 1. Here we represent a quantum system composed of a set of spins with the interaction among them represented by lines. In a fully microscopic description we must take into account all degrees of freedom. (a) In the open quantum system scenario the effective description of a system is given by splitting the microscopic degrees of freedom between into those we have access to, the red spins identified as the system, from those we do not have access to, the blue spins identified as the environment, which are removed by the partial-trace map. (b) In this case the effective description of the underlying microscopic system is given by effective spins, each one related to a coarse-grained detection of two underlying spins. Such a scenario models a situation where we do not resolve any individual microscopic degree of freedom of the system, but we only have access to the effective description that emerges from a blurry detection of the whole system.

given by the uniform average of the states, $\overline{\Omega_\Lambda(\mathcal{O})}^\psi$. The map $\mathcal{A}_\Lambda : \mathcal{O} \mapsto \mathcal{L}(\mathcal{H}_D)$ that takes the known coarse-grained data and assigns to the system a uniform average among all the fine-grained descriptions that agree with the data was named *average assignment map* (AAM) (more details below).

Due to the undeniable importance of the maximum entropy principle in the whole physics, it is the aim of this paper to compare the assignments inferred by the MEP with those inferred by the AAM. Furthermore, we explore the difference between these two assignment maps in a simple thermodynamical process.

II. STATE INFERENCE FROM COARSE-GRAINED DATA

In this section we give further details about the average assignment map, and recall the maximum entropy principle. For both inference methods, we will assume that we have access to an effective system description, living in $\mathcal{L}(\mathcal{H}_d)$, for which we know the coarse-grained data $\mathcal{O} = \{o_i\}$ coming from the expected values of a set $\{O_i\}$ of corresponding effective observables. Moreover, we will use that the system effective description is generated by a coarse-graining map $\Lambda : \mathcal{L}(\mathcal{H}_D) \to \mathcal{L}(\mathcal{H}_d)$.

In the scenario pictured above, notice that a fine-grained state ψ satisfying the coarse-grained constraints $\mathcal{O}$ is in gen-

eral not unique. The set of all fine-grained states in $\mathcal{L}(\mathcal{H}_D)$ that abide by the coarse-grained constraints is then $\Omega_\Lambda(\mathcal{O})$ [see Eq. (1)].

A. Average assignment map (AAM)

From an operational perspective, when assembling an effective preparation ϱ, which is accessed through a coarse-graining map Λ, and with properties $\mathcal{O}$, microscopically we are in fact sampling from the set $\Omega_\Lambda(\mathcal{O})$. Due to the linearity of the expectation value, this perspective suggests an averaging map $\mathcal{A}_\Lambda : \mathcal{O} \rightarrow \mathcal{L}(\mathcal{H}_D)$ that assigns the appropriate description to the microscopic ensemble [32]:

$$\mathcal{A}_\Lambda[\mathcal{O}] \equiv \overline{\Omega_\Lambda(\mathcal{O})}^\psi = \int d\mu_\psi \mathrm{Pr}_\Lambda(\psi|\mathcal{O})\,\psi, \qquad (2)$$

where $d\mu_\psi$ is a prior uniform measure over states in $\mathcal{L}(\mathcal{H}_D)$, and $\mathrm{Pr}_\Lambda(\psi|\mathcal{O})$ is a probability density of having the microscopic state ψ given the macroscopic constraints imposed by $\mathcal{O}$ and the coarse-graining map Λ. Note that $\mathrm{Pr}_\Lambda(\psi|\mathcal{O}) = 0$ for any $\psi \notin \Omega_\Lambda(\mathcal{O})$.

In the particular case where the set $\mathcal{O}$ is big enough as to allow for the full state reconstruction of ϱ in $\mathcal{L}(\mathcal{H}_d)$, that is $\mathcal{O}$ is a tomographically complete set of values, then we can see $\mathcal{A}_\Lambda$ as a map between states, $\mathcal{A}_\Lambda : \mathcal{L}(\mathcal{H}_d) \rightarrow \mathcal{L}(\mathcal{H}_D)$. In this case, that without loss of generality we hereafter concentrate on, the AAM map can be more directly written as

$$\mathcal{A}_\Lambda[\varrho] = \int d\mu_\psi \delta(\Lambda[\psi] - \varrho)\,\psi. \qquad (3)$$

The delta distribution makes clear that all states in $\Omega_\Lambda(\varrho)$ are taken with the same weight in the convex sum.

It is important to discuss the role of the measure μ_ψ. In a situation where the microscopic system is very well isolated, all the ignorance about the system state is classical. In this case, one can consider that the set $\Omega_\Lambda(\varrho)$ contains only pure states, and the measure $d\mu_\psi$ will be the Haar measure over pure states in $\mathcal{H}_D$. However, if the coupling to the environment cannot be neglected, then one needs to include mixed states in $\Omega_\Lambda(\varrho)$, and the choice of the measure μ_ψ is no longer unique. Below we explore different measures, and see how they change the assigned description. The important point, nonetheless, is to realize that the measure μ_ψ allows one to include prior knowledge about the way the system is being prepared.

We used two different methods for calculating the integral in (3) above, the choice of method depending on Λ and μ_ψ. The first method consists in direct calculation of the integral using some representation of the δ (to be described later).

An alternative method takes advantage of the symmetries of Λ, and we briefly introduce it in what follows.

Definition 1. Channel symmetry. Let U be a unitary operator in $\mathcal{L}(\mathcal{H}_D)$. We say that U is a symmetry of Λ if

$$\Lambda[U\psi U^\dagger] = \Lambda[\psi] \qquad (4)$$

for all $\psi \in \mathcal{L}(\mathcal{H}_D)$.

It is sufficient to require that the identity above holds for all pure states, for its validity is extended to all linear operators by linearity. Moreover, it is easy to see that all the symmetries of Λ form a group.

Assume that μ_ψ is unitarily invariant, i.e.,

$$\mu_\psi = \mu_{V\psi V^\dagger} \qquad (5)$$

for all unitary V in $\mathcal{L}(\mathcal{H}_D)$. Then, let U be a symmetry of Λ, and make the change of variables $\psi \rightarrow U\psi U^\dagger$ in Eq. (3), to obtain

$$\mathcal{A}_\Lambda[\varrho] = \int d\mu_\psi \delta(\Lambda[\psi] - \varrho)\,U\psi U^\dagger. \qquad (6)$$

As the assigned state does not change by the application of the symmetry on the fine-grained states, we can average, with an arbitrary measure, over a subset of symmetries and still have the same assignment.

Given that averages are linear functions, we can perform the average over the symmetries before the average over the microstates. In some special cases (we exhibit two examples below) it turns out that such an average over some symmetries presents a remarkable property:

$$\overline{U\psi U^\dagger} = f(\Lambda[\psi]), \qquad (7)$$

with f some function (possibly nonlinear). That is, the average over the symmetries is only a function of the coarse-grained data, as $f(\Lambda[\psi]) = f(\varrho)$. If that is the case, inserting this result into (6), and using the normalization of the measure, we arrive at

$$\mathcal{A}_\Lambda[\varrho] = f(\varrho). \qquad (8)$$

B. Maximum entropy principle (MEP) assignment

As mentioned in the Introduction, the MEP allows for the inclusion of all sorts of constraints. Let $S(\varrho) = -\mathrm{tr}(\varrho \ln \varrho)$ be the von Neumann entropy of a state ϱ. The MEP, taken into account the coarse-grained data $\mathcal{O}$, can be written as

$$\psi_{\mathrm{MEP}} = \arg\max S(\psi)$$
$$\text{s.t. } \mathrm{tr}(O_i \Lambda[\psi]) = o_i, \quad \forall\, i \in \{1, \ldots, |\mathcal{O}|\}. \qquad (9)$$

The above constraints can be equivalently written as $\mathrm{tr}(\Lambda^*[O_i]\psi) = o_i$, where we employed the trace-dual channel associated with the coarse-graining map Λ.

To solve the MEP optimization, it is the standard practice to use the Lagrangian

$$L = -\mathrm{tr}(\psi\,\ln\psi) - \sum_i \lambda_i(\mathrm{tr}(\Lambda^*[O_i]\psi) - o_i), \qquad (10)$$

where λ_i is the Lagrange multiplier associated with the expected value o_i. The state that maximizes the entropy, while satisfying all the constraints, can then be written as

$$\psi_{\mathrm{MEP}} = \frac{1}{Z} \exp\left(-\sum_i \lambda_i \Lambda^*(O_i)\right), \qquad (11)$$

where Z is the partition function, given by $Z = \mathrm{tr}\{\exp[-\sum_i \lambda_i \Lambda^*(O_i)]\}$, as required by the normalization condition of ψ_{MEP}. Finally, the Lagrange multipliers are related to the constraints via the equations:

$$o_i = -\frac{\partial}{\partial\lambda_i}\ln Z, \qquad (12)$$

for all $i \in \{1, 2, \ldots, |\mathcal{O}|\}$.

In the case where $\mathcal{O}$ is sufficient to tomographically reconstruct the effective state $\varrho \in \mathcal{L}(\mathcal{H}_d)$, one can simply write $\text{tr}(O_i \varrho)$ instead of o_i in the expressions above.

III. AAM VS MEP: THREE PHYSICAL SCENARIOS

In what follows we compare the AAM and the MEP assignments for three physical scenarios. The first one is the traditional case of an open quantum system with local constraints; here we want to verify whether the AAM gives the same results as the MEP, as one would expect. For the other two instances the coarse-graining channel cannot be written simply as a partial trace of a subsystem; for these two physical scenarios we expect to see differences between the AAM and MEP assignments, and we explore how such differences may prevail from small to large microscopic systems.

A. Partial trace

In this scenario the total system is described by a density operator in $\mathcal{L}(\mathcal{H}_S \otimes \mathcal{H}_E)$, and the local constraints are described by the system's state $\varrho \in \mathcal{L}(\mathcal{H}_S)$. The full system's description is thus related to the local one via the partial-trace map $\Lambda_{\text{tr}_E} : \mathcal{L}(\mathcal{H}_S \otimes \mathcal{H}_E) \mapsto \mathcal{L}(\mathcal{H}_S)$. In such a situation, the set of fine-grained states that are consistent with the local constraints is then

$$\Omega_{\Lambda_{\text{tr}_E}}(\varrho) = \left\{ \psi \in \mathcal{L}(\mathcal{H}_S \otimes \mathcal{H}_E) \mid \Lambda_{\text{tr}_E}[\psi] = \varrho \right\}.$$

1. AAM assignment

As the trace is basis independent, for any unitary U_E acting on $\mathcal{H}_E$ we have that $\Lambda_{\text{tr}_E}[(\mathbb{1} \otimes U_E)\psi(\mathbb{1} \otimes U_E^\dagger)] = \Lambda_{\text{tr}_E}[\psi]$. The unitary operators of the form $U = \mathbb{1} \otimes U_E$ thus form a symmetry group for Λ_{tr_E}, and we can readily apply the symmetry method to obtain the average assignment for the partial-trace channel. Performing the average over the symmetry group employing the Haar measure we obtain

$$\overline{(\mathbb{1} \otimes U_E)\,\psi\,(\mathbb{1} \otimes U_E^\dagger)} = \Lambda_{\text{tr}_E}[\psi] \otimes \frac{\mathbb{1}_E}{d_E}, \tag{13}$$

with d_E the dimension of $\mathcal{H}_E$. Following the result in Eq. (8), we conclude that

$$\mathcal{A}_{\text{tr}_E}[\varrho] = \varrho \otimes \frac{\mathbb{1}_E}{d_E}. \tag{14}$$

Note that μ_ψ in (6) can be any unitarily invariant measure. Thus, (14) gives the average assignment for the partial-trace channel, both for averages over pure or mixed states.

2. MEP assignment

Since we are assuming to completely know the system's state $\varrho \in \mathcal{L}(\mathcal{H}_S)$, we can consider to know the expectation value of a tomographic set of observables $\{\sigma_i\}$, with $i \in \{x, y, z\}$. For the partial-trace map, we then have $\Lambda_{\text{tr}_E}^*(\sigma_i) = \sigma_i \otimes \mathbb{1}_E$. As such, the state on the total space that maximizes von Neumann's entropy is

$$\psi_{\text{MEP}} = \frac{1}{Z} e^{-\sum_i \lambda_i \sigma_i \otimes \mathbb{1}_E} = \frac{e^{-\sum_i \lambda_i \sigma_i}}{Z_S} \otimes \frac{\mathbb{1}_E}{d_E}, \tag{15}$$

with $Z_S = \text{tr}[\exp(-\sum_i \lambda_i \sigma_i)]$. Nevertheless, as the local system state is fixed by the constraints, we have that the λ_i are

such that

$$\psi_{\text{MEP}} = \varrho \otimes \frac{\mathbb{1}_E}{d_E}. \tag{16}$$

We therefore see that for the partial-trace case, where full knowledge about the system state is given, both the AAM and the MEP assign the same global description for the total system (system+environment).

B. Blurred and saturated detector

Now we introduce our first example of a coarse-graining map that cannot be reduced to the partial trace of a subsystem. The scenario described by the blurred and saturated coarse-graining map Λ_{BnS} is suggested by optical-lattices experiments [33–35]. In such experiments cold atoms are trapped in optical potential wells. Quantum information processing is done by encoding qubits in the atomic energy levels. The readout of information is commonly carried out by a fluorescence technique [36], which for our illustrative purposes can be described, in the single-atom case, as follows: a laser with a well-defined frequency is shone over the atom; if the atom is in the excited state, represented by $|1\rangle$, a rapidly decaying transition is resonantly stimulated and the atom scatters light in all directions; if the atom is the ground state, state $|0\rangle$, the laser is far from resonance, and no light is scattered.

Now imagine that two neighboring atoms are present in the optical lattice, but due to experimental issues it is not possible to distinguish from which atom the light scattered in the fluorescence measurement comes from. In this situation, the two atoms are seen as an effective single two-level atom. The full coarse-graining map modeling this situation is given below (details can be found in [24,29,32,37]):

$$
\begin{aligned}
\Lambda_{\text{BnS}}[|00\rangle\langle 00|] &= |0\rangle\langle 0| & \Lambda_{\text{BnS}}[|10\rangle\langle 00|] &= \frac{1}{\sqrt{3}}|1\rangle\langle 0| \\
\Lambda_{\text{BnS}}[|00\rangle\langle 01|] &= \frac{1}{\sqrt{3}}|0\rangle\langle 1| & \Lambda_{\text{BnS}}[|10\rangle\langle 01|] &= 0 \\
\Lambda_{\text{BnS}}[|00\rangle\langle 10|] &= \frac{1}{\sqrt{3}}|0\rangle\langle 1| & \Lambda_{\text{BnS}}[|10\rangle\langle 10|] &= |1\rangle\langle 1| \\
\Lambda_{\text{BnS}}[|00\rangle\langle 11|] &= \frac{1}{\sqrt{3}}|0\rangle\langle 1| & \Lambda_{\text{BnS}}[|10\rangle\langle 11|] &= 0 \\
\Lambda_{\text{BnS}}[|01\rangle\langle 00|] &= \frac{1}{\sqrt{3}}|1\rangle\langle 0| & \Lambda_{\text{BnS}}[|11\rangle\langle 00|] &= \frac{1}{\sqrt{3}}|1\rangle\langle 0| \\
\Lambda_{\text{BnS}}[|01\rangle\langle 01|] &= |1\rangle\langle 1| & \Lambda_{\text{BnS}}[|11\rangle\langle 01|] &= 0 \\
\Lambda_{\text{BnS}}[|01\rangle\langle 10|] &= 0 & \Lambda_{\text{BnS}}[|11\rangle\langle 10|] &= 0 \\
\Lambda_{\text{BnS}}[|01\rangle\langle 11|] &= 0 & \Lambda_{\text{BnS}}[|11\rangle\langle 11|] &= |1\rangle\langle 1|.
\end{aligned}
\tag{17}
$$

Although inspired by the resonance fluorescence measurement of cold atoms in optical lattices, the above map has no intention to fully capture all the experimental nuances. Nevertheless, it is worth stressing that Λ_{BnS} cannot be reduced to a simple partial trace of one of the subsystems. This can be immediately apprehended by observing the diagonal elements $\Lambda_{\text{BnS}}[|01\rangle\langle 01|] = \Lambda_{\text{BnS}}[|10\rangle\langle 10|] = |1\rangle\langle 1|$: the equalities here are not compatible with the partial trace of either subsystem. For the coherence terms, the $1/\sqrt{3}$ factor is the largest possible while keeping Λ_{BnS} completely positive [24,37].

We then proceed to contrast the AAM and the MEP assignments for this, physically inspired, but not traditionally

described, situation. As for the partial-trace case, we will assume to have a tomographic description of the effective system, i.e., we will assume that to know $\varrho \in \mathcal{L}(\mathcal{H}_2)$, and we want to determine an assignment in $\mathcal{L}(\mathcal{H}_4)$ which abides by the constraints. The set of fine-grained states that are compatible with the effective system is now

$$\Omega_{\Lambda_{\mathrm{BnS}}}(\varrho) = \{\psi \in \mathcal{L}(\mathcal{H}_4) \mid \Lambda_{\mathrm{BnS}}[\psi] = \varrho\}.$$

1. AAM assignment

In what follows we obtain the AAM assignment considering both pure and mixed states in the set $\Omega_{\mathrm{BnS}}(\varrho)$. We start by employing the symmetry method for pure states, and then continue with direct integration for both cases.

a. Symmetry method: pure-state measure. Let $\psi = [\psi]_{ij}$, with $i, j \in \{0, 1, 2, 3\}$, be the matrix representation in the computational basis of a generic state in $\mathcal{L}(\mathcal{H}_4)$, where for the moment we ignore the trace, positivity, and purity constraints that a pure quantum state must fulfill. For the present coarse-graining map, we have

$$\Lambda_{\mathrm{BnS}}[\psi] = \begin{pmatrix} \psi_{00} & \frac{\psi_{01}+\psi_{02}+\psi_{03}}{\sqrt{3}} \\ \frac{\psi_{10}+\psi_{20}+\psi_{30}}{\sqrt{3}} & \psi_{11}+\psi_{22}+\psi_{33} \end{pmatrix}. \quad (18)$$

Using the above expression in the definition of a channel symmetry (4), as we show in Appendix A, the symmetries of Λ_{BnS} can be written as

$$U = \mathbb{1} \oplus \mathbb{1} \oplus V,$$

where the operators on the right-hand side act on the following subspaces: the first subspace is given by the $\mathrm{span}\{|0\rangle\}$, the second one by $\mathrm{span}\{(0, 1, 1, 1)^T/\sqrt{3}\}$, and the third one is an arbitrary two-dimensional subspace orthogonal to the first two. In this way, V is an arbitrary unitary matrix in two dimensions, such that the group of symmetries of Λ_{BnS} is isomorphic to $U(2)$. Following the recipe of the symmetry method ex-

plained above, we chose a parametrization of $V \in U(2)$, and average over the symmetry group to obtain

$$\overline{U\psi U^{\dagger}} = \begin{pmatrix} \bigcirc & \triangle & \triangle & \triangle \\ \triangle^* & \diamond & \square & \square \\ \triangle^* & \square & \diamond & \square \\ \triangle^* & \square & \square & \diamond \end{pmatrix}, \quad (19)$$

where the symbols are given by

$$\bigcirc = \psi_{00}, \quad (20)$$

$$\triangle = \tfrac{1}{3}(\psi_{01} + \psi_{02} + \psi_{03}), \quad (21)$$

$$\diamond = \tfrac{1}{3}(\psi_{11} + \psi_{22} + \psi_{33}), \quad (22)$$

$$\square = \tfrac{1}{6}(\psi_{12} + \psi_{13} + \psi_{23} + \psi_{21} + \psi_{31} + \psi_{32}). \quad (23)$$

Looking at Eq. (18), and imposing $\Lambda_{\mathrm{BnS}}[\psi] = \varrho$, we note that for an arbitrary ψ we must have

$$\bigcirc = \varrho_{00}, \quad \diamond = \frac{\varrho_{11}}{3}, \quad \triangle = \frac{\varrho_{01}}{\sqrt{3}}, \quad (24)$$

where ϱ_{mn}, with $m, n \in \{0, 1\}$, are the matrix coefficients of ϱ in the computational basis.

The $\square$, however, cannot be directly written only in terms of the components of ϱ. If we now assume that ψ is a pure state, then we can write

$$\psi_{ij} = c_i c_j^*, \quad \text{where} \quad |\psi\rangle = (c_0, c_1, c_2, c_3)^T. \quad (25)$$

In this case we have

$$\square = \frac{3\,|\triangle|^2}{2\,\bigcirc} - \frac{\diamond}{2} = \frac{|\varrho_{01}|^2}{2\,\varrho_{00}} - \frac{\varrho_{11}}{6}. \quad (26)$$

Putting all together, when μ_ψ is the uniform measure over pure states, then the average assignment map leads to

$$\mathcal{A}_{\Lambda_{\mathrm{BnS}}}[\varrho] = \begin{pmatrix} \varrho_{00} & \frac{\varrho_{01}}{\sqrt{3}} & \frac{\varrho_{01}}{\sqrt{3}} & \frac{\varrho_{01}}{\sqrt{3}} \\ \frac{\varrho_{01}^*}{\sqrt{3}} & \frac{\varrho_{11}}{3} & \frac{|\varrho_{01}|^2}{2\varrho_{00}} - \frac{\varrho_{11}}{6} & \frac{|\varrho_{01}|^2}{2\varrho_{00}} - \frac{\varrho_{11}}{6} \\ \frac{\varrho_{01}^*}{\sqrt{3}} & \frac{|\varrho_{01}|^2}{2\varrho_{00}} - \frac{\varrho_{11}}{6} & \frac{\varrho_{11}}{3} & \frac{|\varrho_{01}|^2}{2\varrho_{00}} - \frac{\varrho_{11}}{6} \\ \frac{\varrho_{01}^*}{\sqrt{3}} & \frac{|\varrho_{01}|^2}{2\varrho_{00}} - \frac{\varrho_{11}}{6} & \frac{|\varrho_{01}|^2}{2\varrho_{00}} - \frac{\varrho_{11}}{6} & \frac{\varrho_{11}}{3} \end{pmatrix}. \quad (27)$$

It is interesting to realize that in this case the AAM depends in a nonlinear way on the elements of ϱ. This nonlinearity was discussed in greater detail, and applied in an effective communication scenario, in Ref. [25].

b. Explicit integration method: pure-state measure. Before using direct integration to calculate the matrix elements corresponding to $\square$ in Eq. (19) for the case of a mixed-state measure, first we reproduce the pure-state measure result. This will allow us to exhibit the method in simpler setting. After that, the generalization to a mixed-state measure will be relatively straightforward.

In what follows, in order to simplify the calculations' presentation, we employ a hybrid notation for the effective states

$\varrho \in \mathcal{L}(\mathcal{H}_2)$: in part we use its computational basis elements, and in part its Bloch vector representation. Given a fixed effective state ϱ we write it as

$$\varrho = \begin{pmatrix} \varrho_{00} & 0 \\ 0 & \varrho_{11} \end{pmatrix} + \frac{1}{2}(x\,\sigma_x + y\,\sigma_y). \quad (28)$$

In the above expression, σ_i, with $i \in \{x, y, z\}$, are the usual Pauli matrices, $x = \mathrm{tr}(\varrho\,\sigma_x) = 2\,\mathrm{Re}(\varrho_{01})$, and $y = \mathrm{tr}(\varrho\,\sigma_y) = 2\,\mathrm{Im}(\varrho_{01})$.

As we are performing the integration over the pure-state measure (the uniform Haar measure), we directly make use of the pure-state structure, as specified in Eq. (25). The action of the coarse-graining map Λ_{BnS} in a generic pure state can then

be explicitly written as

$$\Lambda_{\text{BnS}}[\psi] = \begin{pmatrix} c_0^* c_0 & c_0(c_1^* + c_2^* + c_3^*)/\sqrt{3} \\ c_0^*(c_1 + c_2 + c_3)/\sqrt{3} & c_1^* c_1 + c_2^* c_2 + c_3^* c_3 \end{pmatrix}.$$
(29)

With the above representations, the average assignment map, Eq. (3), can be expanded as follows for the present case:

$$
\begin{aligned}
\mathcal{A}_{\Lambda_{\text{BnS}}}[\varrho] \propto \int & d\mu_\psi \, \delta(c_0^* c_0 - \varrho_{00}) \\
& \times \delta(c_1^* c_1 + c_2^* c_2 + c_3^* c_3 - \varrho_{11}) \\
& \times \delta(\text{tr}(\Lambda_{\text{BnS}}[\psi] \, \sigma_x) - x) \\
& \times \delta(\text{tr}(\Lambda_{\text{BnS}}[\psi] \, \sigma_y) - y) \, \psi \equiv \mathcal{I},
\end{aligned}
$$
(30)

where $\propto$ indicates that the average state given by the left-hand side, expression, named $\mathcal{I}$, may not be normalized. The normalization constant $\mathcal{N}$ is given by

$$
\begin{aligned}
\mathcal{N} \equiv \int & d\mu_\psi \, \delta(c_0^* c_0 - \varrho_{00}) \\
& \times \delta(c_1^* c_1 + c_2^* c_2 + c_3^* c_3 - \varrho_{11}) \\
& \times \delta(\text{tr}(\Lambda_{\text{BnS}}[\psi] \, \sigma_x) - x) \\
& \times \delta(\text{tr}(\Lambda_{\text{BnS}}[\psi] \, \sigma_y) - y).
\end{aligned}
$$
(31)

The average assignment will then be given as a quotient of two integrals

$$\mathcal{A}_{\text{BnS}}[\varrho] = \frac{\mathcal{I}}{\mathcal{N}}.$$
(32)

Both integrals will be evaluated using the same scheme we now show. The first step is to write the integration measure as a function of the coefficients of $|\psi\rangle = (c_0, c_1, c_2, c_3)^T \equiv c$:

$$d\mu_\psi = \prod_i d\,\text{Re}(c_i) d\,\text{Im}(c_i) \equiv d(c^\dagger, c).$$
(33)

To write the measure as $d(c^\dagger, c)$ is a reminder of its explicit dependence on the complex coefficients c_i. Note that the normalization of $|\psi\rangle$ is implicit in the first two deltas in (30), as long as $\varrho_{00} + \psi_{11} = 1$.

For the present scenario, the effective state ϱ is fixed, and therefore its components in the computational basis ϱ_{ij} are also fixed. Nevertheless, for the sake of calculation we will take them as independent variables. As we are going to perform integral transformations, more specifically Laplace ($\mathfrak{L}$) and Fourier ($\mathfrak{F}$) transformations [38,39], and then take their inverse transformations, their "temporary" independence will be just a calculation artifact. Within this perspective, as ϱ_{00} and ϱ_{11} are positive valued, we can write

$$
\begin{aligned}
\delta(c_0^* c_0 - \varrho_{00}) &= \mathfrak{L}^{-1}\{\mathfrak{L}\{\delta(c_0^* c_0 - \varrho_{00})\}(s_0)\}(\varrho_{00}) \\
&= \mathfrak{L}^{-1}\left\{\int_0^\infty d\varrho_{00} \, e^{-s_0 \varrho_{00}} \delta(c_0^* c_0 - \varrho_{00})\right\}(\varrho_{00}) \\
&= \mathfrak{L}^{-1}\{e^{-s_0 c_0^* c_0}\}(\varrho_{00}).
\end{aligned}
$$
(34)

Similarly, for ϱ_{11},

$$\delta(c_1^* c_1 + c_2^* c_2 + c_3^* c_3 - \varrho_{11}) = \mathfrak{L}^{-1}\{e^{-s_1(c_1^* c_1 + c_2^* c_2 + c_3^* c_3)}\}(\varrho_{11}).$$
(35)

For the remaining components, x and y, as they might assume negative values, we perform Fourier transformations:

$$
\begin{aligned}
& \delta(\text{tr}(\Lambda_{\text{BnS}}[\psi] \, \sigma_x) - x) \\
&\quad = \mathfrak{F}^{-1}\{\mathfrak{F}\{\delta(\text{tr}(\Lambda_{\text{BnS}}[\psi] \, \sigma_x) - x)\}(k_x)\}(x) \\
&\quad = \mathfrak{F}^{-1}\left\{\int_{-\infty}^\infty dx \, e^{-ik_x x} \delta(\text{tr}(\Lambda_{\text{BnS}}[\psi] \, \sigma_x) - x)\right\}(x) \\
&\quad = \mathfrak{F}^{-1}\{e^{-ik_x \text{tr}(\Lambda_{\text{BnS}}[\psi] \, \sigma_x)}\}(x) \\
&\quad = \mathfrak{F}^{-1}\{e^{-ik_x c \, \Lambda_{\text{BnS}}^*[\sigma_x] \, c^\dagger}\}(x).
\end{aligned}
$$
(36)

In the last line we employed the dual channel Λ_{BnS}^*, the definition of $\psi = cc^\dagger$, and the cyclic property of the trace. Proceeding exactly in the same fashion for the y component, we get

$$\delta(\text{tr}(\Lambda_{\text{BnS}}[\psi] \, \sigma_y) - y) = \mathfrak{F}^{-1}\{e^{-ik_y c \, \Lambda_{\text{BnS}}^*[\sigma_y] \, c^\dagger}\}(y).$$
(37)

After transforming all the deltas as shown above, and interchanging the order of integration between the inverse transformations and the integral over states, we can define the Laplace- and Fourier-transformed versions of both $\mathcal{I}$ and $\mathcal{N}$:

$$\tilde{\mathcal{I}}[s_0, s_1, k_x, k_y] = \int d(c^\dagger, c) \, e^{-c^\dagger A c} \, c \, c^\dagger,$$
(38)

$$\tilde{\mathcal{N}}[s_0, s_1, k_x, k_y] = \int d(c^\dagger, c) \, e^{-c^\dagger A c},$$
(39)

where the matrix A is given by

$$A = \text{diag}\,(s_0, s_1, s_1, s_1) + i\Lambda^*[k_x \sigma_x + k_y \sigma_y]$$
(40)

$$= \begin{pmatrix} s_0 & \frac{ik_x + k_y}{\sqrt{3}} & \frac{ik_x + k_y}{\sqrt{3}} & \frac{ik_x + k_y}{\sqrt{3}} \\ \frac{ik_x - k_y}{\sqrt{3}} & s_1 & 0 & 0 \\ \frac{ik_x - k_y}{\sqrt{3}} & 0 & s_1 & 0 \\ \frac{ik_x - k_y}{\sqrt{3}} & 0 & 0 & s_1 \end{pmatrix}.$$
(41)

In this way, the integrals for $\tilde{\mathcal{I}}$ and $\tilde{\mathcal{N}}$ are well-defined Gaussian integrals (as s_0 and s_1 are positive, $A + A^\dagger$ is positive definite), which can be readily performed [40]:

$$\tilde{\mathcal{N}}[s_0, s_1, k_x, k_y] = \frac{\pi^4}{\det A},$$
(42)

$$\tilde{\mathcal{I}}_{ij} = \int d(c^\dagger, c) \, e^{-c^\dagger A c} c_i^* c_j = \frac{\pi^4}{\det A} A_{ji}^{-1},$$
(43)

where A_{ji}^{-1} stands for the ji element of A^{-1}.

The next step is to perform the inverse transforms. Although tedious, this step can be directly performed with the aid of a mathematical software like *Mathematica* [41]. Further details are to be found in Appendix B.

With this final step, all the elements of $\mathcal{A}_{\Lambda_{\text{BnS}}}(\varrho)$, and in particular the one denoted by the $\square$, can be obtained. The result, as expected, is exactly the same as the one shown in Eq. (27).

c. Explicit integration method: mixed-state measure. Up to now, when dealing with the Λ_{BnS} coarse-graining map, we assumed that the set $\Omega_{\Lambda_{\text{BnS}}}(\varrho)$ contained only pure states. Now we deal with the situation where the fine-grained system might be coupled to some other system that we do not have control of, some environment E, and thus all the preparations of our

system of interest in $\mathcal{L}(\mathcal{H}_D)$ are already intrinsically described by a mixed state. In such a situation, there exists no unique uniform measure over mixed states. One way to circumvent this is by employing the unique measure of pure states over the whole space, system, and environment, and trace out the environmental degrees of freedom [42].

Within this mindset, we write

$$\Omega_{\Lambda_{\mathrm{BnS}}}(\varrho) = \{\mathrm{tr}_E(\Psi) \mid \Psi \in \mathcal{L}(\mathcal{H}_D \otimes \mathcal{H}_E),$$

$$\Lambda_{\mathrm{BnS}} \circ \mathrm{tr}_E[\Psi] = \varrho\},$$

with Ψ a pure state in $\mathcal{L}(\mathcal{H}_D \otimes \mathcal{H}_E)$. The average assignment map is then expressed as

$$\mathcal{A}_{\Lambda_{\mathrm{BnS}}}[\varrho] = \int d\mu_\Psi \delta(\Lambda \circ \mathrm{tr}_E[\Psi] - \varrho) \, \mathrm{tr}_E[\Psi], \qquad (44)$$

with $d\mu_\Psi$ the Haar measure over $\mathcal{H}_D \otimes \mathcal{H}_E$. It is important to notice that different environment dimensions will lead to different induced measures of mixed states in $\mathcal{L}(\mathcal{H}_D)$ [42]. This is physically related to "how" open our system of interest is, and its implication will be explored below.

Let $\{|m\rangle\}$, with $m \in \{0, 1, 2, 3\}$, be the computational basis in $\mathcal{H}_D$, and let $\{|\phi_k\rangle\}$, with $k \in \{1, 2, \ldots, d_E\}$, be an orthonormal basis for $\mathcal{H}_E$, whose dimension is d_E. Then, in order to

follow the steps for the pure-measure case, we write

$$|\Psi\rangle = \sum_{k=1}^{d_E} \sum_{m=0}^{3} c_m^k |m\rangle_S \otimes |\phi_k\rangle_E \qquad (45)$$

and evaluate

$$\mathrm{tr}_E |\Psi\rangle\langle\Psi| = \sum_{k=1}^{d_E} \left(\sum_{m=0}^{3} c_m^k |m\rangle \right) \left(\sum_{m'=0}^{3} c_{m'}^{k*} \langle m'| \right)$$

$$\equiv \sum_{k=1}^{d_E} |\psi^k\rangle\langle\psi^k|. \qquad (46)$$

In the above,

$$|\psi^k\rangle = \sum_{m=0}^{3} c_m^k |m\rangle \qquad (47)$$

are subnormalized pure states in $\mathcal{H}_D$. Associating to each pure state $|\psi^k\rangle$ a coordinate vector, i.e., $|\psi^k\rangle \to c^k = (c_0^k, c_1^k, c_2^k, c_3^k)^T$ we can write $\mathrm{tr}_E |\Psi\rangle\langle\Psi| = c^k c^{k\dagger}$, where the summation over repeated indices is assumed whenever it is not explicitly written.

Like in the pure-state measure, we can split the deltas and define

$$\mathcal{A}_{\Lambda_{\mathrm{BnS}}}[\varrho] \propto \int d\mu_\Psi \delta\big(c_0^{k*} c_0^k - \varrho_{00}\big) \delta\big(c_1^{k*} c_1^k + c_2^{k*} c_2^k + c_3^{k*} c_3^k - \varrho_{11}\big) \delta(c^{k\dagger} \Lambda_{\mathrm{BnS}}^* [\sigma_x] c^k - x) \delta(c^{k\dagger} \Lambda_{\mathrm{BnS}}^* [\sigma_y] c^k - y) \, c^{k'} c^{k'\dagger} \equiv \mathcal{I}_{\mathrm{mixed}}, \qquad (48)$$

$$\mathcal{N}_{\mathrm{mixed}} \equiv \int d\mu_\Psi \delta\big(c_0^{k*} c_0^k - \varrho_{00}\big) \delta\big(c_1^{k*} c_1^k + c_2^{k*} c_2^k + c_3^{k*} c_3^k - \varrho_{11}\big) \delta(c^{k\dagger} \Lambda_{\mathrm{BnS}}^* [\sigma_x] c^k - x) \delta(c^{k\dagger} \Lambda_{\mathrm{BnS}}^* [\sigma_y] c^k - y), \qquad (49)$$

where the integration measure now reads as

$$d\mu_\Psi = \prod_{k=1}^{d_E} d(c^{k\dagger}, c^k). \qquad (50)$$

Following the pure-state measure recipe, we now perform the integral transformations to obtain

$$\tilde{\mathcal{I}}_{\mathrm{mixed}} = \sum_{k'=1}^{d_E} \left(\prod_{k=1}^{d_E} \int d(c^{k\dagger}, c^k) \, e^{-c^{k\dagger} A c^k} \right) c^{k'} c^{k'\dagger}$$

$$= d_E \, \tilde{\mathcal{N}}^{d_E - 1} \, \tilde{\mathcal{I}}[s_0, s_1, k_x, k_y] \qquad (51)$$

and

$$\tilde{\mathcal{N}}_{\mathrm{mixed}} = \left(\prod_{k=1}^{d_E} \int d(c^{k\dagger}, c^k) \, e^{-c^{k\dagger} A c^k} \right) \qquad (52)$$

$$= \tilde{\mathcal{N}}^{d_E}[s_0, s_1, k_x, k_y], \qquad (53)$$

with A, $\tilde{\mathcal{N}}$, and $\tilde{\mathcal{I}}$ as in the previous section (pure case).

After doing the inverse transforms (see Appendix B), we arrive at the following result:

$$\Box = \begin{cases} \dfrac{d_E}{3d_E - 1} \dfrac{|\varrho_{01}|^2}{\varrho_{00}} - \dfrac{\varrho_{11}}{3(3d_E - 1)} & \text{mixed states,} \\ \dfrac{|\varrho_{01}|^2}{2\varrho_{00}} - \dfrac{\varrho_{11}}{6} & \text{pure states.} \end{cases} \qquad (54)$$

We included the expression for pure states for the sake of comparison. The pure case corresponds to $d_E = 1$.

In Fig. 2 we show a comparison between pure- and mixed-prior assignments using the trace distance (Δ) as a measure of similarity. We plot the probability density $\mathrm{Pr}(\Delta | d_E)$ of obtaining a distance Δ between the assignments using the pure-state measure and the mixed-state measure, given a fixed environment dimension d_E. An analytical expression for $\mathrm{Pr}(\Delta | d_E)$ is derived in Appendix C, and reads as

$$\mathrm{Pr}(\Delta | d_E) = \frac{3(\Delta - 2a)^2}{8a^3}, \quad 0 \leqslant \Delta \leqslant 2a, \qquad (55)$$

where

$$a = \frac{d_E - 1}{2(3d_E - 1)}. \qquad (56)$$

As expected, and clearly shown in Fig. 2, the probability of large differences between the pure and mixed measures is greater for big environments. In other words, the error that one makes in assuming a closed system, and thus employing a pure-sate measure as prior, is smaller when the environment is small.

2. MEP assignment

To obtain the traditional MEP assignment for the situation described by the blurred and saturated detector coarse-graining map Λ_{BnS}, we start from the general MEP
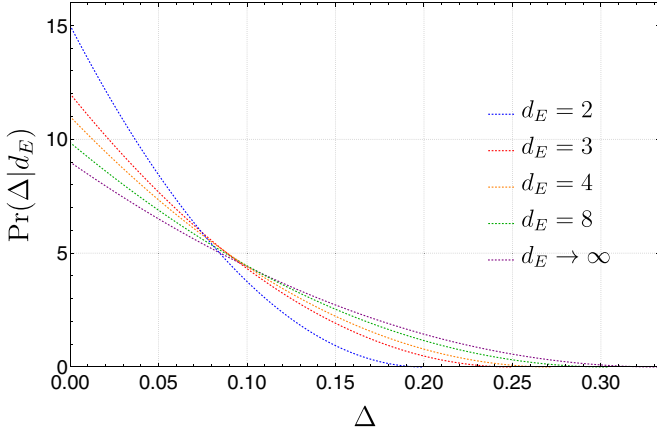
FIG. 2. *Comparison between pure and mixed priors.* The curves represent the probability density $\Pr(\Delta|d_E)$ of obtaining a distance Δ between the pure and mixed assignments, given a fixed environment dimension d_E, when sampling effective states uniformly from the Bloch sphere. According to their probabilities at the origin, the curves correspond to $d_E \in \{2, 3, 4, 8, \infty\}$ ordered from top to bottom.

assignment prescription:

$$\psi_{\text{MEP}}^{\varrho} = \frac{1}{Z} \exp\left(- \sum_{i \in \{x,y,z\}} \lambda_i \Lambda_{\text{BnS}}^{*}[\sigma_i]\right), \qquad (57)$$

with $\Lambda_{\text{BnS}}^{*} : \mathcal{L}(\mathcal{H}_2) \to \mathcal{L}(\mathcal{H}_4)$ the trace-dual map related to Λ_{BnS}. The matrix in the exponent of Eq. (57) can be exactly diagonalized, and then exponentiated.

The ψ_{MEP} for the present scenario has the same structure shown in Eq. (19), but now its elements read as

$$\bigcirc = \frac{1}{Z}\left(\cosh\lambda - \frac{\lambda_z \sinh\lambda}{\lambda}\right), \qquad (58)$$

$$\triangle = -\frac{1}{Z}\left(\frac{(\lambda_x - i\lambda_y)\sinh\lambda}{\sqrt{3}\,\lambda}\right), \qquad (59)$$

$$\square = \frac{1}{3Z}\left(\frac{\lambda_z \sinh\lambda}{\lambda} - e^{\lambda_z} + \cosh\lambda\right), \qquad (60)$$

$$\diamondsuit = \frac{1 - \bigcirc}{3}, \qquad (61)$$

with the partition function given by

$$Z = 2(\cosh\lambda + e^{\lambda_z}). \qquad (62)$$

By imposing the constraint

$$\Lambda\left[\psi_{\text{MEP}}^{\varrho}\right] = \varrho, \qquad (63)$$

we find that the elements denoted by $\bigcirc$, $\diamondsuit$, and $\triangle$ have the same expression as in the case of the average assignment [see Eq. (24)]. However, the elements expressed by a $\square$ are different:

$$\square_{\text{MEP}} = \square_{\text{pure}} - \frac{1}{2Z^2\varrho_{00}}. \qquad (64)$$

Despite the fact that Z is a function of only the effective properties, the effective state ϱ in the present case, we were not able to obtain an analytical expression $Z = Z(\varrho)$, the imposition in Eq. (63), or the equivalent set of equations in (12),
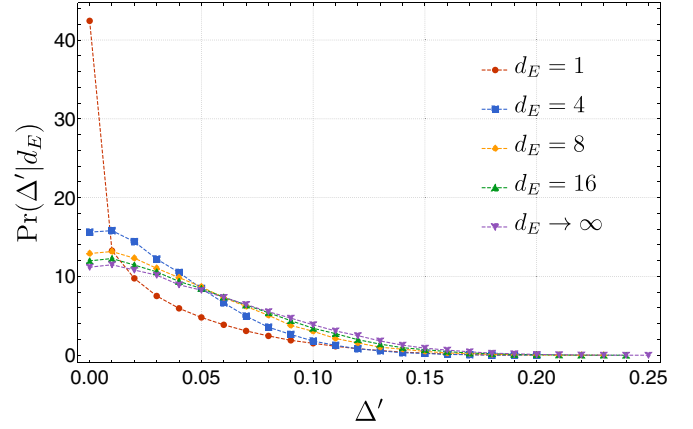

FIG. 3. *Comparison between the MEP and AAM assignments:* Λ_{BnS}. The curves represent the probability density $\Pr(\Delta'|d_E)$ of obtaining a distance Δ' between the MEP and AAM assignments, given a fixed environment dimension d_E, when sampling effective states uniformly from the Bloch sphere. The distance between the MEP and the pure-prior AAM assignment corresponds to $d_E = 1$ (red circles). The distance between the MEP and the mixed-prior AAM assignments are labeled according to the corresponding environmental dimension: $d_E = 4, 8, 16$, and ∞.

lead to transcendental equations. We then resort to numerical evaluations in order to obtain the assigned state by the maximum entropy principle for the situation described by the blurred and saturated detector.

Comparisons between MEP and AAM states, for both pure and mixed priors, are shown in Fig. 3. It is interesting to observe that the probability of small distances ($\Delta' \lesssim 0.02$) between the assigned state by the MEP and the AAM is larger for smaller environment dimension. Further numerical analyses are shown in Appendix E.

C. SU(2)-preserving coarse-graining map

In the previous section we saw that the MEP and the AAM, despite similar guiding principles, may lead to different assigned states. However, the size of the underlying system in the blurred and saturated detector scenario was small, a two spin-$\frac{1}{2}$ system. One may wonder whether such differences still prevail when the dimension of the fine-grained system is much larger than the coarse-grained description.

To address such issue, in this section we exploit the coarse-graining map $\Lambda_J : \mathcal{L}(\mathcal{H}_D) \to \mathcal{L}(\mathcal{H}_2)$ introduced in Ref. [43]. The scenario described by Λ_J is that of a system (that can be a single system, or a collection of subsystems) with total angular momentum J, which is then perceived as an effective single spin-$\frac{1}{2}$ system. The coarse-graining map Λ_J is defined as

$$\Lambda_J[\psi] = \frac{1}{2}\left(\mathbb{1} + \frac{1}{j}\sum_{i\in\{x,y,z\}}\text{tr}(\psi J_i)\,\sigma_i\right), \qquad (65)$$

where J_i are the angular momentum components, i.e., the generators of SU(2) rotations around the x, y, z axes in the D-dimensional Hilbert space $\mathcal{H}_D$, and σ_i are the usual Pauli matrices. In the above expression, j is the largest eigenvalue of J_i, thus fixing $D = 2j + 1$.

An important property of this coarse-graining channel is that it maps a rotated microscopic state in $\mathcal{L}(\mathcal{H}_D)$ to a rotated qubit in $\mathcal{L}(\mathcal{H}_2)$ around the same axis and by the same angle, i.e., Λ_J preserves the SU(2) structure. Mathematically, this invariance is expressed by

$$\Lambda_J[R_{\hat{n}}(\theta)\psi R_{\hat{n}}(\theta)^\dagger] = R'_{\hat{n}}(\theta)\Lambda_J[\psi]R'_{\hat{n}}(\theta)^\dagger, \qquad (66)$$

where $R_{\hat{n}}(\theta) \in \mathcal{L}(\mathcal{H}_D)$ and $R'_{\hat{n}}(\theta) \in \mathcal{L}(\mathcal{H}_2)$ are rotations by an angle θ around a given axis $\hat{n}$:

$$R_{\hat{n}}(\theta) = \exp(-i\theta J_{\hat{n}}), \qquad (67)$$

$$R'_{\hat{n}}(\theta) = \exp(-i\theta \sigma_{\hat{n}}/2), \qquad (68)$$

with $J_{\hat{n}} = \vec{J} \cdot \hat{n}$, $\sigma_{\hat{n}} = \vec{\sigma} \cdot \hat{n}$, and we are setting $\hbar = 1$.

As before, we assume that an effective state ϱ is prepared, and we want to determine which state we should assign to the underlying system. Microscopically, the set of fine-grained states that abide by the constraints is written as

$$\Omega_{\Lambda_J}(\varrho) = \{\psi \in \mathcal{L}(\mathcal{H}_D) \mid \Lambda_J(\psi) = \varrho\}.$$

1. AAM assignment

Before we dive into the evaluation of the AAM assignments (pure and mixed priors), two general observations are in place. First, note that writing ϱ in its Bloch representation,

$$\varrho = \tfrac{1}{2}(\mathbb{1} + \vec{r} \cdot \vec{\sigma}),$$

with $\vec{r} \cdot \vec{\sigma} \equiv r_x \sigma_x + r_y \sigma_y + r_z \sigma_z$, the coarse-graining constraint $\Lambda_J[\psi] = \varrho$ can be expressed as

$$\frac{1}{j}\mathrm{tr}(\psi \vec{J}) = \vec{r}. \qquad (69)$$

Second, notice that if $\psi \in \Omega_{\Lambda_J}(\varrho)$, then $R_{\hat{r}}(\theta)\psi R_{\hat{r}}(\theta)^\dagger$ also belongs to $\Omega_{\Lambda_J}(\varrho)$. This follows from the rotational invariance, Eq. (66), when applied to a rotation around the axis defined by the effective state Bloch vector:

$$\Lambda_J[R_{\hat{r}}(\theta)\psi R_{\hat{r}}(\theta)^\dagger] = R'_{\hat{r}}(\theta)\varrho R'_{\hat{r}}(\theta)^\dagger = \varrho. \qquad (70)$$

Even though $R_{\hat{r}}$ is not a symmetry of Λ_J, as defined in (4) (because it is ψ dependent), the above property simplifies the calculation of average assignments.

This property can be applied in the general form of the AAM assignment, Eq. (3), by making the change of variables $\psi \to R_{\hat{r}}(\theta)\psi R_{\hat{r}}(\theta)^\dagger$, to arrive at

$$\mathcal{A}_{\Lambda_J}[\varrho] = \int d\mu_\psi \delta(\Lambda_J[\psi] - \varrho)R_{\hat{r}}(\theta)\psi R_{\hat{r}}(\theta)^\dagger. \qquad (71)$$

As the assignment in this case, $\mathcal{A}_{\Lambda_J}[\varrho]$, does not depend on θ, we can average over the uniform distribution of rotations around the $\vec{r}$ axis, i.e., we can evaluate $\overline{R_{\hat{r}}(\theta)\psi R_{\hat{r}}(\theta)^\dagger}$ by integrating over $\theta \in [0, 2\pi]$. Although we will not explicitly evaluate such an average, by expressing ψ in the common eigenbasis of $J_{\hat{r}}$ and J^2, which we denote simply by $\{|m_{\hat{r}}\rangle\}$, with $-j \leqslant m \leqslant j$ and where the subindex $\hat{r}$ reminds the basis dependence on the Bloch vector of the effective state, it is

immediate to see that

$$\overline{R_{\hat{r}}(\theta)\psi R_{\hat{r}}(\theta)^\dagger} = \sum_{m,n} \langle m_{\hat{r}}|\psi|n_{\hat{r}}\rangle \overline{e^{-i\theta(m-n)}}^{\mu_\theta}|m_{\hat{r}}\rangle\langle n_{\hat{r}}|$$

$$= \sum_m \langle m_{\hat{r}}|\psi|m_{\hat{r}}\rangle|m_{\hat{r}}\rangle\langle m_{\hat{r}}|.$$

In plain text, just using the invariance property, we determined that the AAM will assign to the fine-grained system a state which is diagonal in the basis $\{|m_{\hat{r}}\rangle\}$. We thus only need to calculate $D = 2j + 1$ averages.

Putting these two observations together, we arrive to the conclusion that the AAM for the coarse-graining map Λ_J can be seen as a function of the effective state ϱ Bloch's vector (due to the rotational symmetry), and that it can be written as

$$\mathcal{A}_{\Lambda_J}[\vec{r}] = \sum_m p_m(r)|m_{\hat{r}}\rangle\langle m_{\hat{r}}|,$$

with $p_m(r) \geqslant 0$ and $\sum_m p_m(r) = 1$ depending only on the modulus $r = |\vec{r}|$ of the Bloch vector due to the rotational symmetry. In what follows, we obtain the p_m coefficients as a function of r.

a. Explicit integration method: pure-state measure. The evaluation of the AAM assigned state now proceeds very closely to the previous calculations. For the present coarse-graining map Λ_J, using the observations above, we write

$$\mathcal{A}_{\Lambda_J}[\vec{r}] \propto \int d\mu_\psi \delta\left(\frac{1}{j}\mathrm{tr}[\psi\vec{J}] - \vec{r}\right)\psi, \qquad (72)$$

where, for the moment, $d\mu_\psi$ is taken as the uniform measure over pure states acting in $\mathcal{L}(\mathcal{H}_D)$.

As the AAM assigned state is diagonal in the common basis of $J_{\hat{r}}$ and J^2, i.e., the basis $\{|m_{\hat{r}}\rangle\}$ defined above, we employ this basis to make the correspondence $|\psi\rangle \to c = (c_1, c_2, \ldots, c_D)^T$, and to write the angular-momentum matrices $\vec{\mathbb{J}}$. The integral above then becomes

$$\mathcal{A}_{\Lambda_J}[\vec{r}] \propto \int d(c^\dagger, c)\,\delta(c^\dagger c - E)\,\delta\left(\frac{1}{j}c^\dagger\vec{\mathbb{J}}c - \vec{r}\right)c\,c^\dagger \equiv \mathcal{I}. \qquad (73)$$

Given that the condition $\mathrm{tr}[\psi\vec{J}] = j\vec{r}$ does not directly impose the normalization of ψ, we explicitly included it with the first δ. In the above, we introduced the variable $E > 0$ for mathematical convenience; at the end of calculations it will be set $E = 1$ [39].

As before, we momentarily take E and $\vec{r}$ as variables. We then perform a Laplace transform, and its inverse, in the normalization condition

$$\delta(c^\dagger c - E) = \mathcal{L}^{-1}\{e^{-s\,c^\dagger c}\}(E),$$

and a Fourier transformation, and its inverse, in the angular momentum constraints

$$\delta\left(\frac{1}{j}c^\dagger\vec{\mathbb{J}}c - \vec{r}\right) = \mathcal{F}^{-1}\{e^{-i\,c^\dagger\vec{k}.\vec{\mathbb{J}}c/j}\}(\vec{r}).$$

In the above, s and $\vec{k} = (k_x, k_y, k_z)$ are the transformation variables.

Exchanging the order of integration between the inverse transforms and the $d(c^\dagger, c)$, we obtain equations analogous to
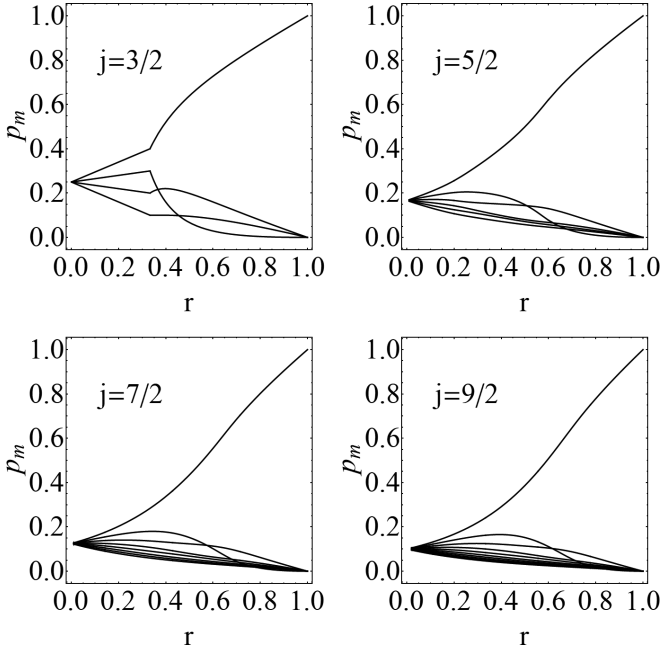
FIG. 4. *Angular momentum distribution for the pure-prior average assignment.* Diagonal elements p_m of $\mathcal{A}_{\Lambda_J}[\varrho]$ are plotted as a function of the parameter r. Each panel refers to a specific value of j: $j = \frac{3}{2}, \frac{5}{2}, \frac{9}{2}, \frac{7}{2}$ in clockwise direction. In all panels, the curves $p_m(r)$ are ordered in decreasing order of m, i.e., the topmost curve corresponds to $m = j$, and the lowest to $m = -j$.

Eqs. (42) and (43):

$$\tilde{\mathcal{I}}_{ij}[s, \vec{k}] = \int d(c^\dagger, c)\, e^{-c^\dagger A c}\, c_i^* c_j = \frac{\pi^D}{\det A} A_{ji}^{-1}, \qquad (74)$$

with the corresponding normalization

$$\tilde{\mathcal{N}}[s, \vec{k}] = \int d(c^\dagger, c^\dagger)\, e^{-c^\dagger A c} = \frac{\pi^D}{\det A}. \qquad (75)$$

For the present case, the matrix A is given by

$$A(s, \vec{k}) = s\mathbb{1} + i\frac{k}{j}\mathbb{J}_{\hat{k}}, \qquad (76)$$

with $\mathbb{J}_{\hat{k}} = \vec{\mathbb{J}} \cdot \hat{k}$.

The next step is to calculate the inverse transforms. We were able to obtain analytical results, but the corresponding expressions are too lengthy to be shown here. Some details are presented in Appendix D. Additionally, Fig. 4 shows the diagonal elements p_m of the pure-prior average assignment $\mathcal{A}_\Lambda[\vec{r}]$ for several values of j.

b. Explicit integration method: mixed-state measure. The evaluation of the AAM for the Λ_J coarse-graining averaging over mixed states proceeds in complete analogy to the case of the blurred and saturated detector (Sec. III B). As in that case, here we express the results for mixed-states average, in terms of the pure-state case. The results are as follows:

$$\tilde{\mathcal{I}}_{\text{mixed}} = d_E \, \tilde{\mathcal{N}}^{d_E - 1} \tilde{\mathcal{I}}[s, \vec{k}] \qquad (77)$$

and

$$\tilde{\mathcal{N}}_{\text{mixed}} = \tilde{\mathcal{N}}^{d_E}[s, \vec{k}], \qquad (78)$$

with A, $\tilde{\mathcal{N}}$, and $\tilde{\mathcal{I}}$ as in the previous section (pure case).
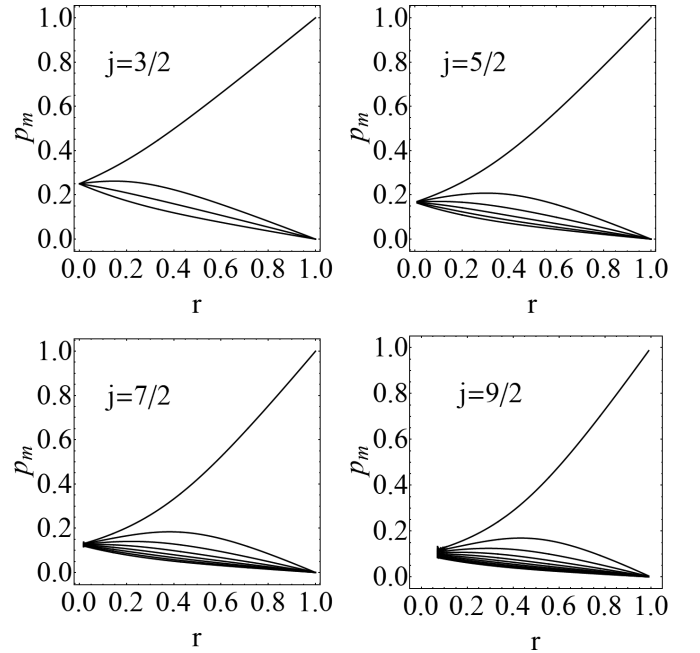

FIG. 5. *Angular momentum distribution for a mixed-prior average assignment.* Diagonal elements p_m of $\mathcal{A}_{\Lambda_J}[\varrho]$ are plotted as a function of the parameter r. The curves in each panel are ordered in decreasing order of m, i.e., the topmost curve corresponds to $m = j$, and the lowest to $m = -j$. For each j value we chose the dimension of the environment d_E to be equal to the system's $D = 2j + 1$.

We present some details about the inverse transformations and final results in Appendix D. Diagonal elements p_m of this assignment as a function of r are plotted in Fig. 5. We chose to show the special case $d_E = D$ because that is the minimal dimension for which any mixed state that satisfies the constraints can be purified.

Some general features of the plots in Figs. 4 and 5 can be readily understood. When $r = 0$, i.e., the effective state is the maximally mixed state, no preferred direction is established. As such, the fine-grained state, for both priors, is the maximally mixed state in $\mathcal{L}(\mathcal{H}_D)$, and thus $p_m(0) = 1/D$ for all m. On the other extreme, when the effective state is a pure state, $r = 1$, then the set $\Omega_{\Lambda_J}(\varrho)$ contains a single state, which is the state with maximum angular momentum in the same direction as the Bloch vector of ϱ, namely, $|m_{\hat{r}}\rangle\langle m_{\hat{r}}|$.

2. MEP assignment

Now we turn our attention to the determination of the state assigned by the maximum entropy principle for the situation described by the coarse-graining map Λ_J. As for the AAM assignment, we assume knowledge of the effective state $\varrho \in \mathcal{L}(\mathcal{H}_2)$. The MEP assignment for this case can then be expressed as the following optimization:

$$\psi^\varrho_{\text{MEP}} = \arg\max S(\psi)$$
$$\text{s.t. } \operatorname{tr}(\sigma_i \Lambda_J[\psi]) = \operatorname{tr}(\sigma_i \varrho) = r_i, \ \forall\, i \in \{x, y, z\}. \quad (79)$$
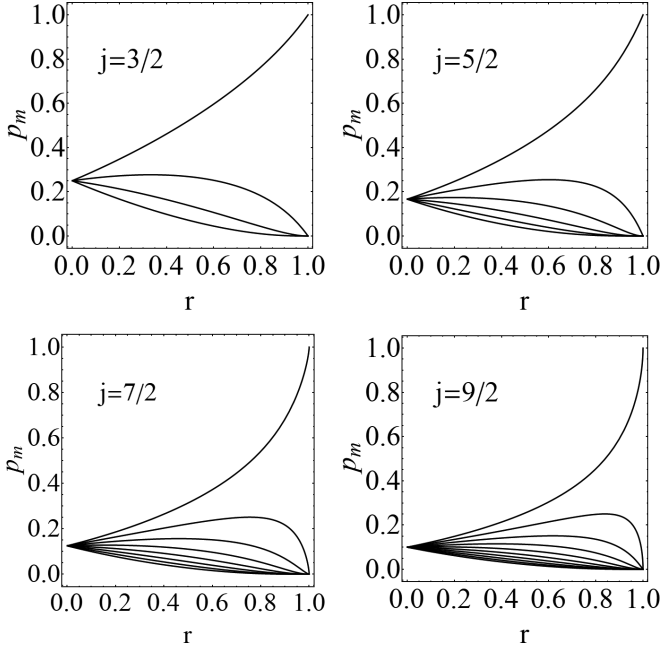
FIG. 6. *Angular momentum distribution for the MEP assignment.* Diagonal elements p_m of $\psi^{\varrho}_{\text{MEP}}$ are plotted as a function of the parameter r. Each one of the subfigures corresponds to a different j value or system's dimension $D = 2j + 1$. All curves $p_m(r)$ are ordered in decreasing order of m, i.e., the upper one corresponds to $m = j$, followed by the curves $m = j - 1, \ldots, m = -j$.

As explained in Sec. II B, under the above constraints, the MEP assignment is given by

$$\psi^{\varrho}_{\text{MEP}} = \frac{1}{Z} \exp\left(-\sum_i \lambda_i \Lambda^*_J[\sigma_i]\right), \tag{80}$$

with the λ_i related to the accessible values via

$$-\frac{\partial}{\partial \vec{\lambda}} \ln Z = \vec{r}. \tag{81}$$

To determine the action of the dual coarse-graining channel on the Pauli matrices, it is sufficient to notice that for any $\psi \in \mathcal{L}(\mathcal{H}_D)$, we have

$$\text{tr}(\Lambda_J[\psi] \sigma_i) = \frac{1}{j} \text{tr}(\psi J_i). \tag{82}$$

It then follows that

$$\Lambda^*[\sigma_i] = \frac{J_i}{j}. \tag{83}$$

That, in fact, is an alternative way of stating the rotational symmetry of Λ_J. Hence, the microscopic state that maximizes the entropy is given by

$$\psi^{\varrho}_{\text{MEP}} = \frac{1}{Z} \exp\left(-\frac{1}{j} \sum_i \lambda_i J_i\right) = \frac{1}{Z} \exp\left(-\frac{1}{j} \lambda J_{\hat{\lambda}}\right), \tag{84}$$

where $J_{\hat{\lambda}} = \vec{J} \cdot \hat{\lambda}$, and λ is the modulus of $\vec{\lambda}$.

Imposing the constraint (81) we obtain

$$-\frac{\partial}{\partial \vec{\lambda}} \ln Z = -\frac{\partial}{\partial \lambda} (\ln Z) \hat{\lambda} = \vec{r}. \tag{85}$$

From the above expression, we see that $\vec{\lambda}$ and $\vec{r}$ are parallel. Without loss of generality, we choose $\hat{\lambda} = -\hat{r}$ and arrive at

$$\psi^{\varrho}_{\text{MEP}} = \frac{1}{Z} \exp\left(\frac{1}{j} \lambda J_{\hat{r}}\right). \tag{86}$$

At the formal level this state is identical to the canonical ensemble of the Brillouin paramagnet [12], with $\vec{\lambda}$ playing the role of the magnetic field $\vec{B} = B\hat{r}$ (modulo some constant). Using this equivalence we can readily write the relation between λ and r:

$$r = \frac{1}{j}\left\{\left(j + \frac{1}{2}\right) \coth\left[\left(j + \frac{1}{2}\right) \frac{\lambda}{j}\right] - \frac{1}{2} \coth \frac{\lambda}{2j}\right\} = \mathcal{B}_j(\lambda), \tag{87}$$

where $\mathcal{B}_j$ is the so-called Brillouin function of jth order.

With the above we have all the elements to construct ψ_{MEP} for the present case. Like for the AAM assignment, the state ψ_{MEP} is diagonal in the eigenbasis of $J_{\hat{r}}$ (and J^2), with matrix elements

$$p_m(r) = \frac{1}{Z} \exp\left(\lambda \frac{m}{j}\right), \tag{88}$$

with $m = -j, -j + 1, \ldots, j - 1, j$, and

$$Z = \frac{\sinh\left[(j + 1/2)\frac{\lambda}{j}\right]}{\sinh\left[\frac{\lambda}{2j}\right]}. \tag{89}$$

Here we did not explicitly show the r dependence of λ to avoid cluttering notation. Thus, the diagonal elements p_m of the MEP assignment can be calculated from Eqs. (87) and (88). The results, for several values of j, are shown in Fig. 6.

Overall, the MEP assignments are similar to the AAM assignments, with the same asymptotic behaviors at $r = 0$ and 1. A quantitative comparison is presented in Fig. 7, where we show the trace distance Δ' between MEP and AAM assigned states as a function of r.

Both cases, pure or mixed prior, are similar, the trace distance being somewhat smaller for the mixed case. However, as the dimension of microscopic system j is increased, Δ' keeps growing, with no sign of slowing down.

In Fig. 7 the environmental dimension was chosen to be $d_E = 2j + 1$, i.e., the same as the system dimension. In Fig. 8 we show that the environment dimension plays no significant role in the distance between the MEP and AAM assignments: a small decrease is observed, but the distance between the assignments is still appreciable, and it seems to saturate for large d_E. Further numerical analyses are shown in Appendix E.

IV. APPLICATION: QUANTUM WORK

In the previous sections we have analyzed different schemes of quantum-state inference from coarse-grained information. This lead to different fine-grained states: the average assignment map (AAM), both pure and mixed priors, and the maximum entropy principle (MEP) assigned states. The aim of this section is to evaluate the observational consequences of these alternative assignments. In what follows, we exploit a thermodynamical process for which we assume that the effective state is given by the SU(2)-preserving coarse-graining map, and inspect the impact of the different
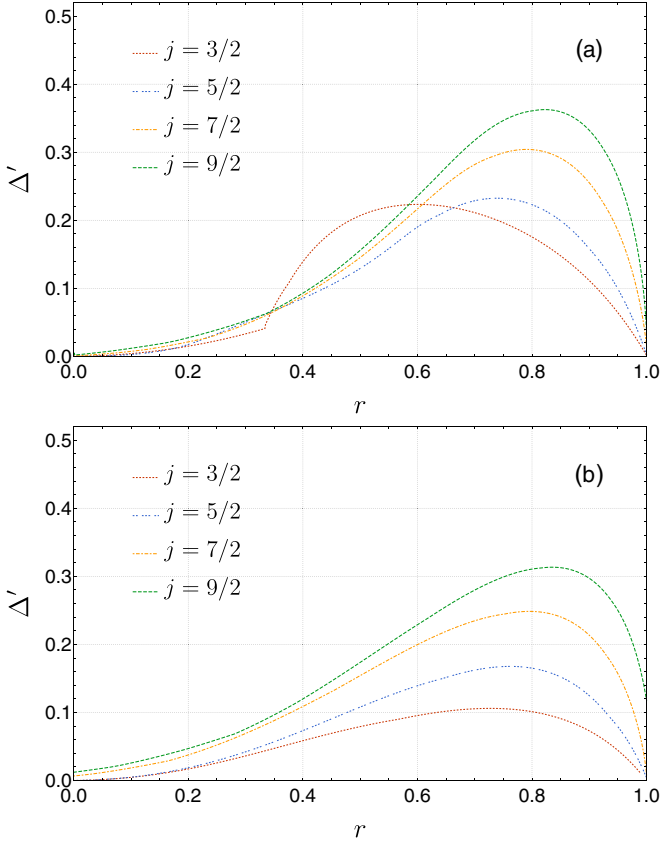
FIG. 7. *Comparison between the MEP and AAM assignments:* Λ_J. (a) Trace distance (Δ') between the MEP and pure-prior AAM assignments is plotted as a function of r. (b) The same as in (a) but for mixed-prior AAM assignment. We consider environmental dimension to be equal to the system's dimension, i.e., $d_E = 2j + 1$. Several values of j are illustrated, $j \in \{\frac{3}{2}, \frac{5}{2}, \frac{7}{2}, \frac{9}{2}\}$, which close to $r = 1$ are ordered from bottom to top.

assignments in the amount of quantum work that can be extracted from the system.

Let us consider a microscopic quantum system composed of a particle, or system of particles, with total angular momentum j, which is thermally isolated. Furthermore, suppose that the underlying dynamics is given by the time-dependent Hamiltonian

$$H(t) = \gamma \, \cos(\omega t) J_z^2, \tag{90}$$

with $\gamma > 0$, and ω an external driving frequency.

Now assume that we have access to this system only via the coarse-graining map Λ_J, defined in (65), with effective initial state given by

$$\varrho_o = \frac{1}{2}(\mathbb{1} + 0.7\sigma_z). \tag{91}$$

This initial state is chosen for two reasons. First, as we can see from Fig. 7, the difference between the AAM and MEP assignments is considerable for all values of j. Second, the AAM and MEP procedures will lead to assigned states which are diagonal in the J_z basis, and as such the assigned states will commute with the Hamiltonian. In this situation the quantum work is uncontroversially defined by [44–47]

$$W = \mathrm{tr}[\overline{\psi}_0 \, (H_F - H_I)], \tag{92}$$
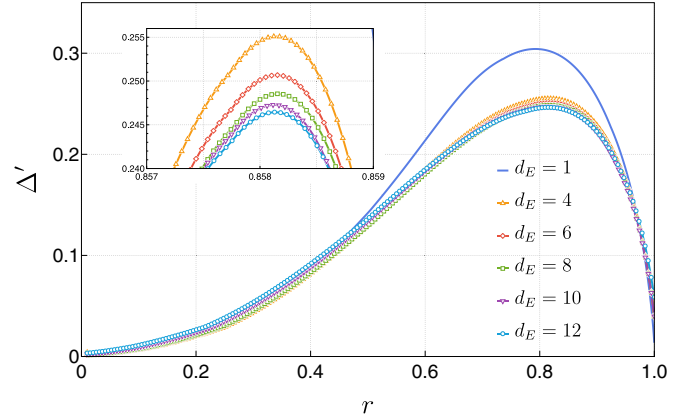

FIG. 8. *Comparison between the MEP and AAM assignments.* Trace distance (Δ') between the MEP and AAM assignments for $j = \frac{7}{2}$ as a function of r. Several environmental dimensions are plotted. The inset shows the saturation of Δ' as the environment's dimension grows.

with $\overline{\psi}_0$ an initial assigned state (AAM pure, AAM mixed, or MEP) and

$$H_I \equiv H(0), \quad H_F = U_\tau^\dagger H(\tau) U_\tau, \tag{93}$$

with U_τ the usual time-ordered evolution operator.

In such a scenario, the average quantum work reads as

$$W = \gamma \, (\cos \omega \tau - 1) \, \mathrm{tr}(\overline{\psi}_0 J_z^2). \tag{94}$$

From the expression above, it is clear that the difference between the assignments will translate into different values of average work. The results for the quantum work are shown in Fig. 9.

It is clear from Fig. 9 that using the MEP assignment always leads to the least amount of work that can be extracted
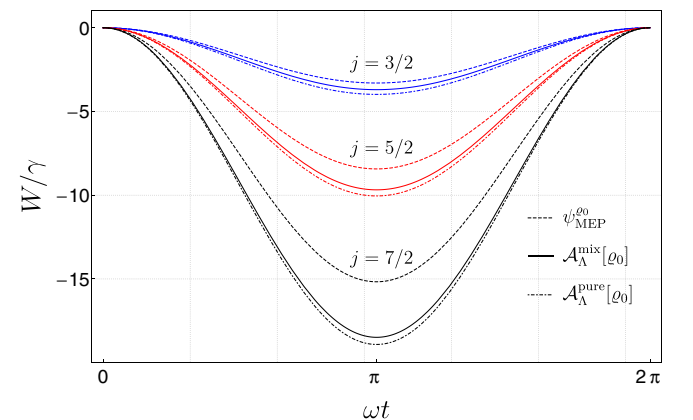

FIG. 9. *Average quantum work for different assignments.* The curves above shown the amount of work that can be extracted from the quantum system when only the effective state is known, for different choices of assignments and different system sizes. For each value of j ($\frac{3}{2}, \frac{5}{2}, \frac{7}{2}$) three assignments are considered: the MEP state (dashed line), the AAM state for a mixed prior ($d_E = 2j + 1$; solid line), and the AAM state for a pure prior (dotted-dashed line). In all the cases, the AAM state over pure states is the one that allows for more work extraction.

from the system. Moreover, among the AAM assignments, to use the average over pure states is always more beneficial, in terms of extracted work, than using the average over mixed states. This ordering can be understood by the knowledge of the physical scenario that each choice entails. While the MEP assignment is fixed given the constraints and the coarse-graining map, for the AAM assignments we still need to specify the measure (the prior) over the microscopic states that abide by the constraints. Choosing a pure state prior is consistent with an experimental setup where the microscopic system is fully isolated. A mixed-state prior with a given environment dimension, on the other hand, assumes some lack of control about the microscopic system and some information about the environment. It is then reasonable to expect that from a situation where a pure-state prior applies, one can extract more work from the quantum system, as it is the situation where more control about the system is present. Of course, using a prior which is not consistent with the experimental situation will lead to a mismatch between the amount of work predicted, and the one in fact extracted or produced.

V. CONCLUSIONS

The maximum entropy principle (MEP) is ubiquitous, and rightly so as it is a cornerstone of thermodynamics and, more generally, of quantum statistical mechanics. Nevertheless, with the rise of complex quantum systems, new scenarios come into play.

Here we analyzed how an assignment map, which shares some foundational ingredients with the MEP, namely, the average assignment map (AAM), behaves in various situations. As expected, in the scenario where only local access to a physical system is granted, the so-called open quantum system picture, both assignments coincide.

However, in situations that go beyond the system-environment split, the two assignment strategies may differ. As we explicitly showed, in the case where two spin-$\frac{1}{2}$ particles, due to experimental constraints, are seen as an effective single spin $\frac{1}{2}$, the two assignments differ [see Eq. (64) and Fig. 3].

As the underlying system is small, two spin-$\frac{1}{2}$ particles, one may expect that such a difference would disappear for larger systems. With the coarse-graining map introduced in Sec. III C, we discredited this possibility. Even for increasing microscopic system dimensions, the difference between the MEP and the AAM assignments remains (see Fig. 7). As it can be seen, the difference in fact increases with the underlying system dimension in this situation.

Where does the difference come from? Both assignments originate from the same idea: there are many microscopic states that abide by some few coarse-grained constraints. If no further constraints are present, the way we evaluate the expectation value of observable quantities in quantum mechanics suggests that a uniform average among all the states that satisfy the constraints is a sensible assignment. The MEP employs an entropic function to obtain such an assignment, with the idea that uniform mixtures maximize the entropy.

The AAM, on the other hand, makes this averaging process explicit. In doing so it becomes evident that a uniform measure over the microscopic states must be chosen. As there is

no unique uniform measure among mixed states, the AAM allows for the introduction of some prior knowledge about the experimental condition: how isolated is the underlying system. If the microscopic system is very well isolated, one can take the average over pure states. If the environmental influence cannot be disregarded, an averaging over mixed states is more judicious. At this point the AAM connects to Bayesian inference methods [48,49], and we show (see, for instance, Figs. 2 and 8) how the assignments differ for each prior knowledge situation. In the above, the only information about the environment employed in the prior was its dimension, but other types of information could be used in a specific scenario.

Finally, when should one use the MEP or the AAM? We showed that depending on the access one has of the system, the assigned states may differ. Using the knowledge about how one accesses the system, and how the system interacts with its environment, if known, can only be beneficial. As different levels of knowledge about an experimental situation are often tied together with more efficient processes, we showed a thermodynamical process where the benefit of employing the AAM assignment is unmistakable (see Fig. 9). The gain of using the AAM assignment, instead of the MEP one, is especially clear in the case where one knows that the system is highly isolated. It should be remarked that choosing an assignment which theoretically would allow for a greater extraction of work, in an experiment scenario which is not befitting with such a choice, will only lead to a poor description and no gain.

APPENDIX A: SYMMETRIES OF Λ_{BnS}

Let us rewrite the definition of symmetry (4) as

$$D \equiv \Lambda[U \chi U^\dagger] - \Lambda[\chi] = 0 \tag{A1}$$

with matrix elements D_{ij}, where $i, j \in \{0, 1\}$. As this identity must hold for all Hermitian matrices $\chi \in \mathcal{L}(\mathcal{H}_4)$, the U-dependent coefficients of D_{ij} must all vanish. From $D_{00} = 0$, and assuming $\text{tr}(\chi) = 1$, we obtain $|U_{00}| = 1$. Unitary then implies that the remaining elements of first column and row are null. Without loss of generality we can set $U_{00} = 1$. Thus, up to now, we have

$$U = \begin{pmatrix} 1 & 0 & 0 & 0 \\ 0 & & & \\ 0 & & \boxed{W} & \\ 0 & & & \end{pmatrix}, \tag{A2}$$

where $W \in U(3)$, with its unitarity guaranteed by the condition $D_{11} = 0$. From requesting $D_{12} = 0$ we obtain the following equations:

$$W_{11} + W_{21} + W_{31} = 1, \tag{A3}$$

$$W_{12} + W_{22} + W_{32} = 1, \tag{A4}$$

$$W_{13} + W_{23} + W_{33} = 1. \tag{A5}$$

This means that W possesses the normalized eigenvector $v_1 = (1, 1, 1)/\sqrt{3}$ with unity eigenvalue, but it is otherwise arbitrary. Then, in a orthonormal basis $\{v_1, v_2, v_3\}$, the matrix W has the structure

$$W = \begin{pmatrix} 1 & 0 & 0 \\ 0 & & \\ 0 & \boxed{V} \end{pmatrix}, \tag{A6}$$

with V an arbitrary unitary in $U(2)$: the arbitrariness of V comes from the freedom in the choice of v_2 and v_3.

The simplest way of calculating the average $\overline{U \chi U}^\dagger$ of Eq. (19) consists in choosing a parametrization of $U(2)$ [50] and then integrating over the parameters.

APPENDIX B: Λ_{BnS} AAM ASSIGNMENT: DETAILS

Our starting point is the quantities $\tilde{\mathcal{N}}$ and $\tilde{\mathcal{I}}$, defined in Eqs. (42) and (43), respectively. These quantities, related to the average over pure states, are the basis also for the mixed case calculations [see Eqs. (51) and (53)].

We begin by doing the inverse transforms in the normalization factor $\tilde{\mathcal{N}}$. The determinant of the matrix A reads as

$$\det A = s_1^2 (k_x^2 + k_y^2 + s_0 s_1) \equiv s_1^2 (\kappa^2 + s_0 s_1), \tag{B1}$$

the last equality defining κ. We first do the Laplace inverse-transform of $\tilde{\mathcal{N}}_{\mathrm{mixed}}$ in the variable s_0:

$$\mathfrak{L}_{s_0}^{-1} \left\{ \frac{\pi^{4d_E}}{(\det A)^{d_E}} \right\}(\varrho_{00}) = \frac{\pi^{4d_E} \varrho_{00}^{d_E - 1} \exp(-\kappa^2 \varrho_{00}/s_1)}{s_1^{3d_E} \Gamma(d_E)}. \tag{B2}$$

Then, we Laplace inverse-transform the right-hand side above in s_1:

$$\mathfrak{L}_{s_1}^{-1}\{\ldots\}(\varrho_{11}) = \frac{\pi^{4d_E} \varrho_{11}^{(3d_E - 1)/2} J_{3d_E - 1}(2\kappa \sqrt{\varrho_{00}\varrho_{11}})}{\kappa^{3d_E - 1} \varrho_{00}^{(d_E + 1)/2} \Gamma(d_E)}, \tag{B3}$$

where $J_{3d_E - 1}$ is a Bessel function. Now we must do the inverse Fourier transforms on the last expression. Note that such expression only depends on the polar radius κ in the plane (k_x, k_y). Using $r_\perp = \sqrt{x^2 + y^2}$, we have

$$\mathcal{N}_{\mathrm{mixed}}(\varrho) = \int dk_x \, dk_y \, e^{i(k_x x + k_y y)}(\ldots) \tag{B4}$$

$$= 2\pi \int_0^\infty dk \, \kappa \, J_0(\kappa r_\perp)(\ldots) \tag{B5}$$

$$= \frac{2^{4(1-d_E)} \pi^{4d_E + 1} (1 - r^2)^{3d_E - 2}}{\Gamma(d_E)\Gamma(3d_E - 1)(1 + z)^{2d_E}}, \tag{B6}$$

where we have made the substitutions $\varrho_{00/11} \to (1 \pm z)/2$, used $x^2 + y^2 + z^2 = r^2$, and $(\ldots)$ stands for the right-hand side of Eq. (B3).

In the following we apply the same succession of inverse transforms as above (in the same order) to $\tilde{\mathcal{I}}_{\mathrm{mixed}}$. We focus on the six elements denoted with a square in Eq. (19), as those, for the mixed prior, cannot be calculated using the symmetry method. If we choose, say, $\mathcal{A}_{\Lambda, 23}$ as a representative, we must inverse-transform $\tilde{\mathcal{I}}_{\mathrm{mixed}, 23}$. Combining Eqs. (42), (43), and (51), we obtain

$$\tilde{\mathcal{I}}_{\mathrm{mixed}, 23} = d_E \left(\frac{\pi^4}{\det A} \right)^{d_E} A_{32}^{-1} \tag{B7}$$

$$= \frac{d_E \, \pi^{4d_E}}{(\det A)^{d_E + 1}} C_{23}, \tag{B8}$$

where C_{23} is the appropriate cofactor of A, which reads as

$$C_{23} = -\frac{\kappa^2 s_1}{3}. \tag{B9}$$

The first Laplace inverse-transform, in the variable s_0, gives

$$\mathfrak{L}_{s_0}^{-1}\{\tilde{\mathcal{I}}_{\mathrm{mixed}, 23}\}(\varrho_{00}) = -\frac{\pi^{4d_E} \kappa^2 \varrho_{00}^{d_E} \exp(-\kappa^2 \varrho_{00}/s_1)}{3 \, \Gamma(d_E) s_1^{2(d_E + 1)}}. \tag{B10}$$

Transforming the expression above, now in s_1, produces

$$\mathfrak{L}_{s_1}^{-1}\{\ldots\}(\varrho_{11}) = -\frac{\pi^{4d_E} \varrho_{11}^{(3d_E + 1)/2} J_{3d_E + 1}(2\kappa \sqrt{\varrho_{00}\varrho_{11}})}{3 \, \kappa^{3d_E - 1} \varrho_{00}^{(d_E + 1)/2} \Gamma(d_E)}. \tag{B11}$$

Now we calculate the inverse Fourier transform of the last expression:

$$\mathcal{I}_{\mathrm{mixed}, 23}(\varrho)$$
$$= \frac{d_E 2^{3 - 4d_E} \pi^{4d_E - 1}(1 - r^2)^{3d_E - 2}[3d_E(x^2 + y^2) + z^2 - 1]}{3 \, \Gamma(d_E + 1)\Gamma(3d_E)(1 + z)^{2d_E + 1}}. \tag{B12}$$

Finally, forming the quotient $\mathcal{I}/\mathcal{N}$, we recover the result of Eq. (54):

$$\mathcal{A}_{\Lambda, 23}(\varrho) = \frac{3d_E(x^2 + y^2) + z^2 - 1}{6(3d_E - 1)(z + 1)} \tag{B13}$$

$$= \frac{d_E}{3d_E - 1} \frac{|\varrho_{01}|^2}{\varrho_{00}} - \frac{\varrho_{11}}{3(3d_E - 1)}. \tag{B14}$$

APPENDIX C: DISTANCE BETWEEN $\mathcal{A}_{\Lambda_{\mathrm{BnS}}}^{\mathrm{mixed}}$ AND $\mathcal{A}_{\Lambda_{\mathrm{BnS}}}^{\mathrm{pure}}$

The trace distance is just half of the trace norm of the difference of the matrices:

$$\Delta(\varrho, \sigma) = \tfrac{1}{2}||\varrho - \sigma||_1 = \tfrac{1}{2}\mathrm{tr}[\sqrt{(\varrho - \sigma)^\dagger(\varrho - \sigma)}]. \tag{C1}$$

The purpose of the factor of 2 is to restrict the trace distance between two normalized density matrices to the range [0, 1]. Since density matrices are Hermitian,

$$\Delta(\varrho, \sigma) = \frac{1}{2} \sum_i |\lambda_i|, \tag{C2}$$

where the λ_i are eigenvalues of the Hermitian, but not necessarily positive, matrix $(\varrho - \sigma)$.

The trace distance between average (over pure or mixed states) assignments can be calculated from Eq. (54). The dif-

ference between assignments has the following structure:

$$\mathcal{A}_{\Lambda_{\mathrm{BnS}}}^{\mathrm{mixed}}[\varrho] - \mathcal{A}_{\Lambda_{\mathrm{BnS}}}^{\mathrm{pure}}[\varrho] = \begin{pmatrix} 0 & 0 & 0 & 0 \\ 0 & 0 & \mu & \mu \\ 0 & \mu & 0 & \mu \\ 0 & \mu & \mu & 0 \end{pmatrix}. \quad (C3)$$

From Eq. (54) we obtain

$$\mu = \frac{(d_E - 1)(1 - r^2)}{4(3d_E - 1)(1 + z)}. \quad (C4)$$

The eigenvalues of the difference matrix (C3) are $\{2\mu, -\mu, -\mu, 0\}$. Then, the trace distance Δ is

$$\Delta = 2\mu = \frac{(d_E - 1)(1 - r^2)}{2(3d_E - 1)(1 + z)}. \quad (C5)$$

In order calculate the probability distribution of Δ we must compute the following integral over the Bloch ball:

$$\mathrm{Pr}(\Delta | d_E) = \frac{3}{4\pi} \int dx\, dy\, dz\, \delta(\Delta - 2\mu(x, y, z; d_E)), \quad (C6)$$

which leads to Eq. (55).

APPENDIX D: Λ_J AAM ASSIGNMENTS: DETAILS

In the case of the present coarse graining it is not possible to obtain general formulas of the average assignments for arbitrary j and d_E. Each case must be handled separately. In the following we show some details of the calculation of the inverse Fourier and Laplace transforms of the quantities $\tilde{\mathcal{I}}$ and $\tilde{\mathcal{N}}$, whose quotient $\mathcal{I}(\vec{r})/\mathcal{N}(\vec{r})$ determines the average assignment.

We start by calculating the norm $\mathcal{N}(\vec{r})$. The determinant (76) reads as

$$\det A = \prod_{m=-j}^{j} \left(s + \frac{ikm}{j} \right). \quad (D1)$$

Note that $\det A$ is even function of k. We do first the inverse Fourier transform of $\tilde{\mathcal{N}}(s, \vec{k})$. As $\det A$ only depends on $k = |\vec{k}|$, it is convenient to use spherical coordinates in $\vec{k}$ space; without loss of generality, we choose $\hat{z} = \hat{r}$. Then, the Fourier transform is given by

$$\mathcal{N}_{\mathrm{mixed}}(s, \vec{r}) = \frac{4\pi^{Dd_E + 1}}{r} \int_0^\infty dk\, \frac{k\, \sin(kr)}{(\det A)^{d_E}}. \quad (D2)$$

Next, we Laplace transform:

$$\mathcal{N}_{\mathrm{mixed}}(\vec{r}) = \mathfrak{L}_s^{-1}\{\mathcal{N}_{\mathrm{mixed}}(s, \vec{r})\}(E)|_{E=1}. \quad (D3)$$

By virtue of the SU(2) symmetry, the norm only depends on the modulus of $\vec{r}$, for all j and d_E. We show one example, for $j = \frac{3}{2}$ and $d_E = 2$:

$$\mathcal{N}_{\mathrm{mixed}}(s, r) = \frac{27\pi^{10} e^{-3rs}}{128\, rs^6} [2rs + e^{2rs}(6rs - 3) + 3], \quad (D4)$$

$$\mathcal{N}_{\mathrm{mixed}}(r) = \frac{9\pi^{10}}{5120 r} [3(1 - 3r)^5 \theta(1 - 3r)$$
$$+ 10r(1 - 3r)^4 \theta(1 - 3r) + 3(r - 1)^5$$
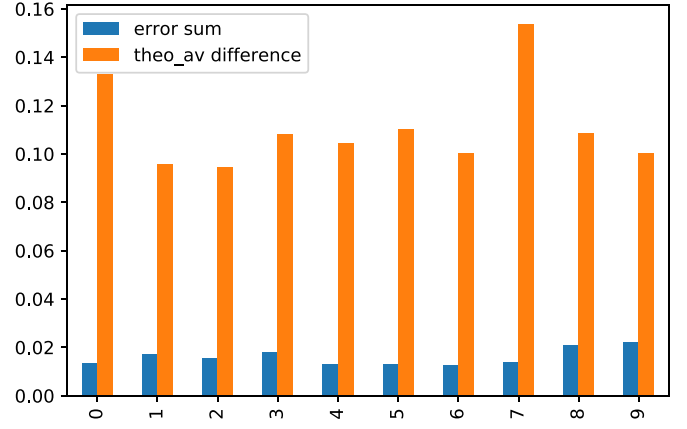$$+ 30(r - 1)^4 r]. \quad (D5)$$

FIG. 10. *Rejection sampling analyses of preparation errors:* Λ_{BnS}. The blue bars above (left bars for each state) denote the total error $||\mathcal{A}_\Lambda^{\epsilon,\mathrm{pure}}[\varrho] - \mathcal{A}_\Lambda^{\mathrm{pure}}[\varrho]||_1 + ||\mathcal{A}_\Lambda^{\epsilon,\mathrm{mixed}}[\varrho] - \mathcal{A}_\Lambda^{\mathrm{mixed}}[\varrho]||_1$, while the orange bars quantify the distance between the error-free analytical results $||\mathcal{A}_\Lambda^{\mathrm{pure}}[\varrho] - \mathcal{A}_\Lambda^{\mathrm{mixed}}[\varrho]||_1$. The horizontal axis represents the index of the effective state (see Table I).

As j and/or d_E are increased, the expressions above grow rapidly, though preserving the structure: $\mathcal{N}_{\mathrm{mixed}}(r)$ is a sum of Heaviside theta functions multiplied by polynomials of r; the theta functions increase in number with j, the polynomials increase in degree with j and d_E.

Now, let us turn to $\tilde{\mathcal{I}}_{\mathrm{mixed}}$. Using Eqs. (75) and (74) into (77), we arrive at

$$\tilde{\mathcal{I}}_{\mathrm{mixed},mm}(s, \vec{k}) = d_E\, \pi^{d_E D} \frac{C_{mm}}{(\det A)^{d_E + 1}}. \quad (D6)$$

We have observed that C_{mm}, the diagonal cofactors of A, do not depend on the azimuthal angle ϕ; then, the inverse Fourier transform reads as

$$\tilde{\mathcal{I}}_{\mathrm{mixed},mm}(s, r) = 2d_E\, \pi^{d_E D + 1} \int_0^\infty dk\, \frac{k^2}{(\det A)^{d_E + 1}}$$
$$\times \int_0^\pi d\theta\, \sin\theta\, \exp(ikr\cos\theta)\, C_{mm}. \quad (D7)$$

The last step consists in inverse-transforming Laplace ($s \to E$) the expression above, and setting $E = 1$. The result $\mathcal{I}_{\mathrm{mixed},mm}(r)$ has the same structure as the norm $\mathcal{N}_{\mathrm{mixed}}(r)$, but appreciably more complex. Finally, dividing $\mathcal{I}_{\mathrm{mixed},mm}(r)$ by $\mathcal{N}_{\mathrm{mixed}}(r)$ we obtain the probabilities $p_m(r)$ plotted in the Figs. 4 and 5.

APPENDIX E: FURTHER NUMERICAL ANALYSIS: Λ_{BnS} AND Λ_J

In the main text we showed that, for a fixed coarse-graining map Λ and fixed effective state ϱ, the assignments when employing pure or mixed priors are in general different, with the exception of the partial-trace map. This conclusion can be visually apprehended, for instance, from Figs. 2 and 7. For Λ_{BnS} the analytical evaluation of the trace distance between $\mathcal{A}_{\Lambda_{\mathrm{BnS}}}^{\mathrm{pure}}(\varrho)$ and $\mathcal{A}_{\Lambda_{\mathrm{BnS}}}^{\mathrm{mixed}}(\varrho)$ is presented in Appendix C.

In the above discussion it was, nevertheless, assumed that the effective state ϱ could be perfectly prepared, which of course is not the case in a realistic scenario. Two points
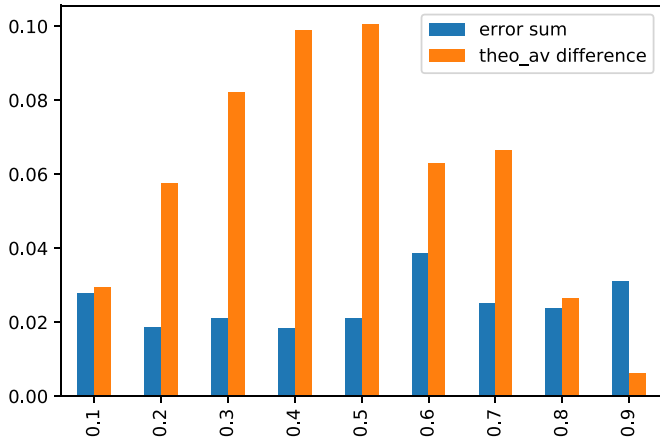
FIG. 11. *Rejection sampling analyses of preparation errors: Λ_{BnS}.* The blue bars above (left bars for each state) denote the total error $||\mathcal{A}_\Lambda^{\epsilon,\text{pure}}[\varrho] - \mathcal{A}_\Lambda^{\text{pure}}[\varrho]||_1 + ||\mathcal{A}_\Lambda^{\epsilon,\text{mixed}}[\varrho] - \mathcal{A}_\Lambda^{\text{mixed}}[\varrho]||_1$, while the orange bars quantify the distance between the error-free analytical results $||\mathcal{A}_\Lambda^{\text{pure}}[\varrho] - \mathcal{A}_\Lambda^{\text{mixed}}[\varrho]||_1$. The horizontal axis represents the Bloch vector length r of the effective state.

could then be raised: (i) How close is the error-free analytical assignment $\mathcal{A}_\Lambda$ from the one obtained when preparation errors are allowed? (ii) Does the difference between the assigned states for pure and mixed priors prevail when errors in the preparation of ϱ are allowed?

To address these points, we extended the definition of the set of states that abide by the constraints, as to allow for a preparation error ϵ:

$$\Omega_\Lambda^\epsilon(\varrho) = \{\psi \in \mathcal{L}(\mathcal{H}_D) \mid ||\Lambda(\psi) - \varrho||_1 \leqslant \epsilon\}. \quad (\text{E1})$$

We then proceed by the way of a simple rejection sampling algorithm: for fixed ϱ, Λ, and ϵ, we uniformly sampled a large number (to be specified later) of states in $\mathcal{L}(\mathcal{H}_D)$ and checked which ones belong to $\Omega_\Lambda^\epsilon(\varrho)$. With the ones that are selected, we estimate the assigned state with preparation error ϵ as the average state $\mathcal{A}_\Lambda^\epsilon[\varrho] = \overline{\Omega_\Lambda^\epsilon(\varrho)}$.

Numerically, we generated a database of 10^6 pure 2-qubit states, and 10^6 pure 3-qubit states, sampled from their respective Haar measure. These databases were used both for Λ_{BnS} and $\Lambda_{J=3/2}$. With the 2-qubit sample we obtained $\mathcal{A}_{\Lambda_{\text{BnS}}}^{\epsilon,\text{pure}}$ and $\mathcal{A}_{\Lambda_{J=3/2}}^{\epsilon,\text{pure}}$ for selected effective states (see below). With the database of 3 qubits, after performing the partial trace on the third qubit, we estimated $\mathcal{A}_{\Lambda_{\text{BnS}}}^{\epsilon,\text{mixed}}$ and $\mathcal{A}_{\Lambda_{J=3/2}}^{\epsilon,\text{mixed}}$. In all cases we set the preparation error as $\epsilon = 0.025$.

Figures 10 and 11 summarize the obtained results. In both plots, the blue bars (left bar for each point in the

TABLE I. Effective states used in the rejection sampling algorithm to obtain the assigned states in the Λ_{BnS} case when preparation error is allowed.

Index	$\text{tr}(\varrho\sigma_x)$	$\text{tr}(\varrho\sigma_y)$	$\text{tr}(\varrho\sigma_z)$
0	-0.3061	0.1269	-0.6142
1	0.0923	0.1550	0.0119
2	-0.0776	0.1248	0.03211
3	-0.2439	0.0130	-0.1526
4	0.0749	0.0032	-0.0502
5	-0.1384	0.1779	-0.1613
6	-0.1082	-0.1748	-0.0468
7	-0.1021	0.0914	-0.5838
8	-0.1434	-0.1630	-0.1391
9	0.3696	-0.0652	-0.1729

horizontal axis) quantify the total difference between the analytical expression and the ones obtained numerically, i.e., for each ϱ it equals $||\mathcal{A}_\Lambda^{\epsilon,\text{pure}}[\varrho] - \mathcal{A}_\Lambda^{\text{pure}}[\varrho]||_1 + ||\mathcal{A}_\Lambda^{\epsilon,\text{mixed}}[\varrho] - \mathcal{A}_\Lambda^{\text{mixed}}[\varrho]||_1$. The orange bars (right bar for each point in the horizontal axis) quantify the difference between the pure and mixed prior analytical states for each ϱ, i.e., $||\mathcal{A}_\Lambda^{\text{pure}}[\varrho] - \mathcal{A}_\Lambda^{\text{mixed}}[\varrho]||_1$.

This choice of presentation allows us to address both raised points. From the small values obtained for the blue bars we observe that the analytical error-free results are close to the ones when preparation errors are allowed. By comparing the height of the orange bars with the blue ones, we appreciate that the estimated average states with error are closer to their respective analytical result than the distance between the analytical results for pure and mixed priors. In other words, the pure- and mixed-prior assigned states could be distinguished even if preparation errors are allowed.

As can be seen from the plot for Λ_{BnS} (Fig. 10), for all randomly selected states (see Table I) the total error is always much smaller than the difference between the error-free analytical results. That confirms that when preparation errors are allowed, the assigned state does not change appreciably, and that pure- and mixed-prior assignments can be distinguished.

For Λ_J, Fig. 11, as expected, the difference between the error-free pure and mixed priors is small for almost pure effective states ($r \simeq 1$) and highly mixed effective states ($r \simeq 0$). For such cases, the preparation error might not permit the distinction between pure- and mixed-prior assignments. This distinction is, however, possible for intermediate purity effective states. In all the cases, given the small size of the blue bars, the assigned states when $\epsilon = 0.025$ are close to the ones when $\epsilon = 0$.

[1] E. T. Jaynes, Information theory and statistical mechanics, Phys. Rev. **106**, 620 (1957).

[2] E. T. Jaynes, Information theory and statistical mechanics. ii, Phys. Rev. **108**, 171 (1957).

[3] J. R. Banavar, A. Maritan, and I. Volkov, Applications of the principle of maximum entropy: From physics to ecology, J. Phys.: Condens. Matter **22**, 063101 (2010).

[4] J. Karmeshu, *Entropy Measures, Maximum Entropy Principle and Emerging Applications*, Vol. 119 (Springer, New York, 2003).

[5] J. Harte, *Maximum Entropy and Ecology: A Theory of Abundance, Distribution, and Energetics* (Oxford University Press, Oxford, 2011).

[6] W. Boomsma, J. Ferkinghoff-Borg, and K. Lindorff-Larsen, Combining experiments and simulations using the maxi-

mum entropy principle, PLoS Comput. Biol. **10**, e1003406 (2014).

[7] A. De Martino and D. De Martino, An introduction to the maximum entropy approach and its application to inference problems in biology, Heliyon **4**, e00596 (2018).

[8] A. Cesari, S. Reißer, and G. Bussi, Using the maximum entropy principle to combine simulations and solution experiments, Computation **6**, 15 (2018).

[9] A. L. Berger, S. A. Della Pietra, and V. J. Della Pietra, A maximum entropy approach, *Natural Language Processing*, Computational Linguistics, Vol. 22 (MIT Press, Cambridge, MA, 1996), pp. 39–71.

[10] A. K. Bera and S. Y. Park, Optimal portfolio diversification using the maximum entropy principle, Econometric Rev. **27**, 484 (2008).

[11] A. Caticha and A. Golan, An entropic framework for modeling economies, Phys. A (Amsterdam) **408**, 149 (2014).

[12] R. K. Pathria and P. D. Beale, *Statistical Mechanics* (Academic, New York, 2011).

[13] V. Bužek, R. Derka, G. Adam, and P. L. Knight, Reconstruction of quantum states of spin systems: From quantum Bayesian inference to quantum tomography, Ann. Phys. **266**, 454 (1998).

[14] V. Bužek, Quantum tomography from incomplete data via maxent principle, in *Quantum State Estimation*, Lecture Notes in Physics (Springer, Berlin, 2004), Chap. 6, pp. 189–234.

[15] A. O. Caldeira and A. J. Leggett, Influence of Dissipation on Quantum Tunneling in Macroscopic Systems, Phys. Rev. Lett. **46**, 211 (1981).

[16] H.-P. Breuer and F. Petruccione, *The Theory of Open Quantum Systems* (Oxford University Press, Oxford, 2002).

[17] N. D. Mermin, Quantum mechanics vs local realism near the classical limit: A bell inequality for spin *s*, Phys. Rev. D **22**, 356 (1980).

[18] D. Poulin, Macroscopic observables, Phys. Rev. A **71**, 022102 (2005).

[19] J. Kofler and Č. Brukner, Conditions for Quantum Violation of Macroscopic Realism, Phys. Rev. Lett. **101**, 090403 (2008).

[20] S. Raeisi, P. Sekatski, and C. Simon, Coarse Graining Makes it Hard to See Micro-Macro Entanglement, Phys. Rev. Lett. **107**, 250401 (2011).

[21] T. Wang, R. Ghobadi, S. Raeisi, and C. Simon, Precision requirements for observing macroscopic quantum effects, Phys. Rev. A **88**, 062114 (2013).

[22] H. Jeong, Y. Lim, and M. S. Kim, Coarsening Measurement References and the Quantum-To-Classical Transition, Phys. Rev. Lett. **112**, 010402 (2014).

[23] J. Park, S.-W. Ji, J. Lee, and H. Nha, Gaussian states under coarse-grained continuous variable measurements, Phys. Rev. A **89**, 042102 (2014).

[24] C. Duarte, G. D. Carvalho, N. K. Bernardes, and F. de Melo, Emerging dynamics arising from coarse-grained quantum systems, Phys. Rev. A **96**, 032113 (2017).

[25] P. Silva Correia and F. de Melo, Spin-entanglement wave in a coarse-grained optical lattice, Phys. Rev. A **100**, 022334 (2019).

[26] O. Kabernik, Quantum coarse graining, symmetries, and reducibility of dynamics, Phys. Rev. A **97**, 052130 (2018).

[27] C. Duarte, Compatibility between agents as a tool for coarse-grained descriptions of quantum systems, J. Phys. A: Math. Theor. **53**, 395301 (2020).

[28] I. Veeren and F. de Melo, Entropic uncertainty relations and the quantum-to-classical transition, Phys. Rev. A **102**, 022205 (2020).

[29] G. D. Carvalho and P. S. Correia, Decay of quantumness in a measurement process: Action of a coarse-graining channel, Phys. Rev. A **102**, 032217 (2020).

[30] C. Duarte, B. Amaral, M. T. Cunha, and M. Leifer, Investigating coarse-grainings and emergent quantum dynamics with four mathematical perspectives, arXiv:2011.10349.

[31] C. Pineda, D. Davalos, C. Viviescas, and A. Rosado, Fuzzy measurements and coarse graining in quantum many-body systems, Phys. Rev. A **104**, 042218 (2021).

[32] P. S. Correia, P. C. Obando, R. O. Vallejos, and F. de Melo, Macro-to-micro quantum mapping and the emergence of nonlinearity, Phys. Rev. A **103**, 052210 (2021).

[33] C. Gross and I. Bloch, Quantum simulations with ultracold atoms in optical lattices, Science **357**, 995 (2017).

[34] I. Bloch, Quantum coherence and entanglement with ultracold atoms in optical lattices, Nature (London) **453**, 1016 (2008).

[35] T. Fukuhara, S. Hild, J. Zeiher, P. Schauß, I. Bloch, M. Endres, and C. Gross, Spatially Resolved Detection of a Spin-Entanglement Wave in a Bose-Hubbard Chain, Phys. Rev. Lett. **115**, 035302 (2015).

[36] J. F. Sherson, C. Weitenberg, M. Endres, M. Cheneau, I. Bloch, and S. Kuhr, Single-atom-resolved fluorescence imaging of an atomic mott insulator, Nature (London) **467**, 68 (2010).

[37] O. Duranthon and G. Di Molfetta, Coarse-grained quantum cellular automata, Phys. Rev. A **103**, 032224 (2021).

[38] V. Laliena, Effect of angular momentum conservation in the phase transitions of collapsing systems, Phys. Rev. E **59**, 4786 (1999).

[39] A. Lakshminarayan, S. Tomsovic, O. Bohigas, and S. N. Majumdar, Extreme Statistics of Complex Random and Quantum Chaotic States, Phys. Rev. Lett. **100**, 044103 (2008).

[40] A. Altland and B. D. Simons, *Condensed Matter Field Theory* (Cambridge University Press, Cambridge, 2010).

[41] Wolfram Research, Inc, Wolfram programming lab, Version 13.0.0, https://www.wolfram.com/programming-lab.

[42] K. Zyczkowski and H.-J. Sommers, Induced measures in the space of mixed quantum states, J. Phys. A: Math. Gen. **34**, 7111 (2001).

[43] I. Saideh, A. D. Ribeiro, G. Ferrini, T. Coudreau, P. Milman, and A. Keller, General dichotomization procedure to provide qudit entanglement criteria, Phys. Rev. A **92**, 052334 (2015).

[44] F. Binder, L. A. Correa, C. Gogolin, J. Anders, and G. Adesso, *Thermodynamics in the Quantum Regime*, Vol. 195 (Springer, Berlin, 2018).

[45] M. Campisi, P. Hänggi, and P. Talkner, Colloquium: Quantum fluctuation relations: Foundations and applications, Rev. Mod. Phys. **83**, 771 (2011).

[46] A. E. Allahverdyan, Nonequilibrium quantum fluctuations of work, Phys. Rev. E **90**, 032137 (2014).

[47] P. Talkner, E. Lutz, and P. Hänggi, Fluctuation theorems: Work is not an observable, Phys. Rev. E **75**, 050102(R) (2007).

[48] C. M. Caves, C. A. Fuchs, and R. Schack, Quantum probabilities as bayesian probabilities, Phys. Rev. A **65**, 022305 (2002).

[49] R. Blume-Kohout, Optimal, reliable estimation of quantum states, New J. Phys. **12**, 043034 (2010).

[50] K. Zyczkowski and M. Kus, Random unitary matrices, J. Phys. A: Math. Gen. **27**, 4235 (1994).